SNOW DEPTH ESTIMATION USING DIFFERENT SAR IMAGE MODALITIES

TISHYA DUGGAL

June, 2024

SUPERVISORS:

Dr. ing. Hossein Aghababaei
Dr. Ling Chang

SNOW DEPTH ESTIMATION USING DIFFERENT SAR IMAGE MODALITIES

Tishya Duggal
Enschede, The Netherlands, June 2024

Thesis submitted to the Faculty of Geo-Information Science and Earth Observation of the University of Twente in partial fulfilment of the requirements for the degree of Master of Science in Geo-information Science and Earth Observation.
Specialization: Geoinformatics

SUPERVISORS:
Dr. ing. Hossein Aghababaei
Dr. Ling Chang

THESIS ASSESSMENT BOARD:
Prof. dr. ir. Claudio Persello (Chair)
Dr. Lu Zhou (External Examiner, University of Utrecht)

ABSTRACT:

Estimating snow depth is vital for various purposes like hydrology, climate modelling, avalanche risk assessment, and winter sports. While remote sensing techniques, particularly Synthetic Aperture Radar (SAR), have made significant advancements in estimating snow depth, there remains a lack of comparative assessments of various SAR modalities. This includes employing different polarization modes, frequencies, and sensor platforms for accurate snow depth estimation over complex terrains. This study thus employs SAR data from various platforms, including Sentinel-1, SAOCOM, and UAVSAR, to investigate the impacts of different polarisation configurations (dual polarimetric (DP) and quad polarimetric (QP)), different frequencies (C- and L- bands), and different SAR sensor platforms (airborne and spaceborne) on snow depth estimation. The study focuses on five sites situated in the mountainous terrains of the western USA. By utilizing NASA's SnowEx snow depth data as a reference and employing a Random Forest regression model, this study reports a comparative assessment of SAR-based snow depth estimation performance across polarization, frequency, and sensor platforms. The results indicated varying degrees of accuracy among the different SAR datasets, with UAVSAR operating as an airborne system in quad-polarised mode and its L-band frequency consistently achieving the best performance across most study areas, exhibiting the lowest RMSE and MAE values. Following it, spaceborne SAOCOM's quad-polarimetric L-band data performed notably well but still with higher RMSE and MAE values than UAVSAR. Next in line, dual-polarimetric spaceborne data from both Sentinel-1 (C-band, 10 m spatial resolution) and SAOCOM (L-band, 50 m spatial resolution) often showed comparable error levels, with Sentinel-1 achieving slightly lower RMSE and MAE values amongst the two datasets due to an advantage of higher spatial resolution. Overall, the SAOCOM dual-polarimetric dataset yielded the least accurate results across most study areas. Visual inspection of the maps revealed that the UAVSAR predictions had the closest resemblance to the reference snow depth maps among all other datasets. The models struggled to predict the full range of snow depth values accurately thus leading to a compressed range of values in the predicted maps. The difference maps indicated that large errors were mainly concentrated in regions with extreme snow depth values, where the models tended to underestimate the higher values and overestimate the lower values.

Keywords
Snow depth, Synthetic Aperture Radar (SAR), Machine Learning, Random Forest, Polarization, Frequency

ACKNOWLEDGMENTS:

I would like to express my deepest gratitude to all the people who have contributed to the completion of my thesis. Without their guidance, patience, and unwavering support, this journey would not have been possible.

First and foremost, I am profoundly grateful to my first supervisor, Dr. Hossein Aghababaei. His constant support has been invaluable. Dr. Aghababaei was always ready to provide guidance and assistance, no matter how small or complex the problem. He also encouraged me to present this thesis at a conference. This achievement wouldn't have been possible without his constant belief in my abilities. His dedication and willingness to help me through every step of this research made all the difference, and for that, I am deeply thankful. This thesis wouldn't have been possible without his supervision, and I couldn't have asked for a better supervisor.

I would also like to extend my heartfelt thanks to my second supervisor, Dr. Ling Chang. Her insights, feedback, and expertise have greatly enriched this research. Her constructive criticism pushed me to strive for excellence and has significantly contributed to the quality of this work.

My sincere thanks go to Dr. Andreas Dietz, my supervisor during my internship at the Team of Cold and Polar Regions, German Aerospace Center (DLR). His expertise in this field, along with his support and mentorship, provided me with invaluable experience and knowledge. I am also grateful to the entire team at DLR for their collaboration and encouragement during my time there.

I am eternally grateful to my parents and my sister, who have always been my pillars of strength. Their unwavering love, support, and belief in me have been my greatest motivation. To my friends Sanaa and Ayushi, who, despite being miles away, have been a constant source of support and encouragement throughout these two challenging years. Your friendship has been my source of comfort and strength.

I would also like to thank all my dearest friends at ITC. Your friendship has made this journey enjoyable and memorable. A special mention goes to Uzzi, whose companionship and support have been invaluable. Special thanks to my senior, Rddhi, whose guidance, and advice have been immensely helpful during this master's degree.

Lastly, I would like to thank God for giving me the strength, patience, and perseverance to complete this thesis.

This journey has been both challenging and rewarding, and I am grateful to all those who have been a part of it. Your contributions have been invaluable, and this work would not have been possible without you. Thank you all from the bottom of my heart.

TABLE OF CONTENTS

LIST OF FIGURES

LIST OF TABLES

CHAPTER 1

Introduction

1.1. Background

Water is undoubtedly the most vital natural resource for human beings and ecosystems all around the planet. Considering the problems posed by climate change, monitoring water resources is essential (Muelchi et al., 2021). During the summer, water stored as snow is critical for over a billion people globally (Lievens et al., 2019). Snow, an essential part of the Earth's cryosphere, contributes significantly to the hydrological cycle, climate systems, and other environmental processes (T. G. F. Kittel et al., 2011). Therefore, estimating snow depth has garnered significant scientific and practical importance.

The seasonal heavy snowfall is known to cause disruptions in transportation, agriculture, infrastructure, and ecosystems. Snow-related hazards like avalanches often pose life-threatening risks to humans (Schweizer et al., 2003). Snow depth or snow thickness can be defined as the distance of the snow surface to the ground. Snow depth estimation (SDE) is imperative for assessing avalanche risk and improving its forecasting (Bühler et al., 2022). This information can help conduct efficient mitigation measures and guarantee the safety of populations living in snow-prone areas. In colder areas, the water collected in snowpacks during the winter melts and flows off in the summer. Rapid melting of snow can sometimes cause rivers to overflow and result in flooding (Bashmakov et al., 2022). Contrarily, some areas (e.g., the Alpine region) depend entirely on this meltwater for domestic, agricultural, and commercial use during the summer (Lievens et al., 2022). However, global warming and climate change mess with the dynamics of snowmelt and consequently alter the quantity and timing of available water, remarkably through the concept of Snow Water Equivalent (SWE) (Lievens et al., 2022). The knowledge of SWE and hydrological processes can be strengthened by monitoring the depth of snow. Moreover, SDE can advance our knowledge of climate systems and how climate change affects snow regimes (Li et al., 2022). It enables researchers to examine trends, variations, and shifts in the snowpack's properties by keeping track of changes in snow depth. Accurate SDE is crucial for developing climate and weather forecasting models, especially in areas impacted by extreme winter weather conditions. Thus, extensive knowledge of snow depth and how it changes with the climate is critical for managing water supplies and supporting a sustainable future for communities.

1.2. Literature Review

Historically, territorial techniques such as manual surveys and in-situ measurements using mechanical instruments were used for the prediction of the parameters of snow, such as its depth, density, and albedo (Gallet et al., 2009; Montpetit et al., 2012; Worby et al., 2008). While they offer accurate data, these methods are labour-intensive, time-consuming, and have limited

availability due to low spatial coverage and are unfeasible in isolated areas such as very high mountain peaks (Li et al., 2022). LiDAR (Light Detection and Ranging) is one of the most widely utilised methods for research on snow and the whole cryosphere (Leinss et al., 2014; Tedesco et al., 2014). It employs laser pulses to gauge the distance between the LiDAR sensor and the top surface of the snow as well as the Earth's surface (Baños et al., 2011). LiDAR is appropriate for snow mapping because it can deliver high-resolution, three-dimensional topography data, which is relevant for SDE and snow mapping (Broxton et al., 2019). Deems et al. (2013) predicted snow depth from airborne LiDAR data quite accurately. However, the study also depicted that weather conditions strongly influence LiDAR data; for example, heavy rainfall or snowfall can scatter and absorb laser beams. Additionally, the cost of acquiring and processing airborne LiDAR data limits its availability to many researchers. Optical remote sensing methods, over the years, have successfully utilised visible and near-infrared wavelengths for detecting and monitoring the snow cover (Cannistra et al., 2021; Vikhamar & Solberg, 2003). This approach offers worldwide coverage, is economical, and is non-invasive. However, these conclusions were confined to the snowpack's surface because it is difficult to precisely estimate snow depth due to the inability of optical remote sensing wavelengths to penetrate the snow cover (Varade & Dikshit, 2018, 2019). Moreover, there are several drawbacks to optical remote sensing, including reliance on daylight and cloud cover. For comprehensive research on the snow's depth, Synthetic Aperture Radar (SAR) gained fame for being beneficial over optical remote sensing, owing to the microwave signal's increased penetrability (Kelly et al., 2003; Ulaby & Long, 2015).

SAR has emerged as effective for providing spatially distributed and comprehensive information on the depth of snow cover on the Earth (Qiao et al., 2023a). The study by Che et al. (2008) presented how SAR data can be employed to generate reliable conclusions about snow depth. SAR data also advantageously allows the study of large areas. However, at present, most of the studies with large-scale estimates of snow depth, such as of complete mountain ranges, have a low spatial resolution (Lievens et al., 2019, 2022; Muñoz-Sabater et al., 2021; Saha et al., 2010). Contrastingly, high resolution is considered important for SDE because it can capture greater details (Cimoli et al., 2017). Since it is impossible to track snow depth over the whole cryosphere at high spatial resolution, such studies are only helpful for understanding snow depth at the planetary scale. Thus, they are useless in smaller and specific areas, e.g., the Himalayan or Alpine terrain, because they cannot capture their spatial diversity. Qiao et al. (2023) developed a snow profile reconstruction method based on Unmanned Aerial Vehicle (UAV) SAR tomography, primarily including spectral estimation-based 3D imaging methods and a snow profile correction. Using a UAV provided high resolution but restricted the study to a small scale. Such small-scale models using airborne platforms that can span only a small area have drawbacks because they have not been tested for different regions or complex topographies and are too expensive to scale over vast areas (Bühler et al., 2015; Eberhard et al., 2021).

Zhou et al. (2018) investigated the retrieval of snow depth along with sea ice thickness using a combination of L-band remote sensing data and laser altimetry. Empirical models were developed to estimate snow depth and sea ice thickness in the Beaufort Sea in the Arctic region. The study highlighted a significant relationship between snow depth and snow freeboard and incorporated this covariability into a retrieval algorithm to improve the accuracy of the retrievals. The study successfully achieves reliable retrievals of snow depth and sea ice thickness, with major errors arising mainly from mismatches between modelled and observed data. Moreover, the research demonstrated the potential of L-band microwave radiation's ability to penetrate through snow and facilitate the tracking of snow dynamics in polar

locations. Recent advancements in the retrieval of snow depth and SWE have also used dual-polarization X-band SAR data. Patil et al. (2020) demonstrated the effectiveness of using co-polar phase difference (CPD) and particle anisotropy models for accurate snow depth and SWE inversion, validated by field measurements. Most recently, Daudt et al. (2023) presented a state-of-the-art technique for estimating snow depth using SAR data at a high spatial resolution (10 m) with a recurrent convolutional neural network (CNN). This method yielded rare findings for large-scale and high-resolution snow depth mapping with decent accuracy. The outcomes were compared to high-fidelity snow depth maps acquired using aircraft laser-scanning for three years to assess the accuracy. The study did, however, notice model-induced abnormalities and uncertainties in the snow depth estimates of various locations, such as the absence of features or the presence of under-represented objects in the resulting maps. SDEs have been generated with moderate accuracy and have achieved reasonable success in the past, but such products are uncommon and rely on either enormous ground monitoring networks or the integration of SAR data with other datasets (Wulf et al., 2020).

1.3. Research Gap and Problem

Although research on snow depth assessment using radar remote sensing has advanced significantly, there are still several research gaps in existing knowledge. Most of the current research works compromised on resolution of the study. Although SAR is fundamentally designed for distance-based data acquisition, the backscattering coefficients of SAR imagery vary systematically with snow depth due to changes in surface and volume scattering properties (Patil et al., 2020). Thus, accurately deriving snow depth from SAR backscatter, especially in mountainous terrains, poses a significant challenge due to the complex interplay of topography, snow properties, and SAR signal characteristics. Moreover, there is a lack of comparative analyses on SDE using different polarisations, frequencies, and spatial resolutions. Comprehensive knowledge of how the variations in these characteristics influence the accuracy of SDE remains unexplored. Notably, less research has been done on machine learning models that can estimate snow depth while considering complex terrains. Furthermore, higher accuracies of snow depth estimations have mostly been attained by combining radar remote sensing data with field observations of snow depth (Guneriussen et al., 2001; Varade et al., 2019). Thus, there is room for further research to quantify the potential of SAR alone for SDE. These research gaps must be filled by precise and robust analysis that can quantify the performance of SAR-based SDEs operating on different sensor modalities for any terrain type without relying on auxiliary data. This research leverages advanced machine learning techniques to address the intricacies of snow depth retrieval from SAR backscatter data, aiming to enhance the precision and reliability of SDE in these challenging environments. By using remotely sensed SAR data provided by Sentinel-1, SAOCOM and UAVSAR, the research aims to evaluate the snow depth estimated from different SAR modalities, including differences in frequency, polarization, and sensor platforms, in order to identify the most accurate and reliable approaches for SDE. By utilising UAVSAR, this research also allows for estimating snow depth at high resolutions. The study aims to improve the accuracy and reliability of SAR-based snow depth estimations by bridging the existing knowledge gap between incompetent models of the current state-of-the-art and highly accurate models.

1.4. Research Objectives and Questions

1.4.1. Main Objective

The main objective of this study is to estimate snow depth using various SAR modalities, including different SAR frequencies (C- and L- bands), different SAR sensor platforms (airborne and spaceborne), and different polarisation configurations (dual polarimetric and quad polarimetric). Furthermore, the accuracy of these snow depth estimations will be assessed, and a comparison of their respective machine-learning models will be conducted.

1.4.2. Sub-Objectives

1. To estimate snow depth values using C-band dual-polarimetric spaceborne SAR dataset.
2. To estimate snow depth values using L-band quad-polarimetric airborne SAR dataset.
3. To estimate snow depth values using L-band quad-polarimetric spaceborne SAR dataset.
4. To estimate snow depth values using L-band dual-polarimetric spaceborne SAR dataset.

1.4.3. Research Questions

RQ1: Which frequency (C-band or L-band) of SAR will result in a more accurate estimation of snow depth?

RQ2: Do the SDE accuracies differ across airborne SAR and spaceborne SAR when the same frequency (L-band) is used?

RQ3: Which of the polarisation modalities (quad-polarisation or dual-polarisation) results in a more accurate estimation of snow depth?

1.5. Thesis Structure

The rest of this thesis comprises four additional chapters: 'Study Area, Datasets, and Tools' (Chapter 2), 'Methodology' (Chapter 3), 'Experimental Results and Discussion' (Chapter 4) and 'Conclusion' (Chapter 5). Chapter 2 introduces the study area and datasets used while Chapter 3 details the proposed methodology for this research. Chapter 4 presents the experimental results of this study which are also discussed thoroughly. Finally, Chapter 5 concludes the thesis.

CHAPTER 2

Study Area, Datasets, and Tools

2.1. Study Area

The United States of America is a geographically diverse nation, having a wide range of climatic conditions and landscapes. As shown in Figure 1, the study areas for this research are located in the western parts of the USA, within the hilly terrains of Fraser and Cameron Pass in Colorado, Little Cottonwood Canyon in Utah, and Basin Summit and Mores Creek in Idaho. Refer to Table 1 for the latitudinal and longitudinal extents of the research sites. These regions make up an important part of the Rocky Mountain range and encompass mountains located at elevations ranging from 4,000 to 14,000 feet above sea level (F. Kittel et al., 2002). These areas have a frigid climate, with wintertime temperatures occasionally falling below zero degrees due to their high altitudes (Sospedra-Alfonso et al., 2015). The five study area sites might have diverse microclimates and weather conditions due to their varying geographies, but one common characteristic is that they all experience chilly winters with significant snowfall. The snowfall generally begins in late October and lasts far into April (Sospedra-Alfonso et al., 2015). Moreover, the high elevations and freezing weather conditions collectively contribute to the prolonged snowpack in these areas during the winter months (Beniston et al., 2003). Thus, the interplay of temperature and terrain with snowfall significantly influences the dynamics of snow accumulation in the focussed study areas, providing an ideal environment for SDE research.

Table 1: Latitudinal and Longitudinal extent of the study area

SPATIAL EXTENT	FRASER, COLORADO	CAMERON PASS, COLORADO	LITTLE COTTONWOOD CANYON, UTAH	BASIN SUMMIT, IDAHO	MORES CREEK, IDAHO
Northernmost Latitude	39° 55' 55.1078" N	40° 34' 20.4826" N	40° 35' 53.8023" N	44° 20' 32.9025" N	43° 58' 59.7560" N
Southernmost Latitude	39° 50' 12.2667" N	40° 30' 16.0790" N	40° 31' 13.3951" N	44° 11' 39.9990" N	43° 54' 28.4898" N
Easternmost Longitude	105° 50' 48.5365" W	105° 51' 41.7900" W	111° 36' 55.2166" W	115° 5' 19.5890" W	115° 38' 11.3655" W
Westernmost Longitude	105° 56' 33.8299" W	105° 55' 3.1991" W	111° 43' 13.0314" W	115° 16' 47.5332" W	115° 44' 3.4585" W

Figure 1: Study Area Map displaying the locations of the five study area sites

2.2. Data Sources

This study employs SAR imageries from Sentinel-1, UAVSAR (Uninhabited Aerial Vehicle Synthetic Aperture Radar) and SAOCOM (Satélite Argentino de ObservaciónCOnMicroondas) to estimate Snow Depth using machine learning algorithms. The SnowEx20-21 Snow Depth dataset provides snow depth values at five distinct sites in the western USA and will be used as the reference dataset to train the models. These models will be used to predict snow depth for all the sites using SAR imageries. The acquisition date of the SnowEx LIDAR dataset was March 2021 when all the study areas were mostly covered by snow during this period. The SAR datasets mentioned in Table 2, including Sentinel-1, UAVSAR and SAOCOM imagery, were also collected for either the same or around the same timeframe to ensure environmental consistency and temporal relevance while comparing their models' performances.

2.2.1. SnowEx Snow Depth Dataset

NASA SnowEx is a multi-year project aimed at improving estimates and measurements of snow-surface energy balance and snow water equivalent (SWE). This campaign aims to combine modelling, in-situ observations, and remote sensing to find the best method for snow monitoring and to identify ways to achieve precise snow measurements taken from space (Marshall et al., 2020). The SnowEx20-21 snow depth dataset (SnowEx20-21 QSI Lidar Snow Depth 3m UTM Grid, Version 1 | National Snow and Ice Data Center) used in this study is a component of the SnowEx 2020 and SnowEx 2021 campaigns. The source of this dataset is a point cloud digital terrain model (PCDTM). The team generated a PCDTM during snow-free conditions and later generated a PCDTM during snow-covered conditions. The snow depth was then derived by differencing these measurements during "snow-on" and "snow-off" conditions (McGrath et al., 2019). This dataset is freely available on NASA's Earthdata portal in the form of raster images (see Figure 2) providing pixel-wise snow depth values at a 3 m spatial resolution. For this study, five georeferenced images containing snow depth information including, 1) Basin Summit and 2) Mores Creek in Idaho, 3) Cameron Pass and 4) Fraser in Colorado, and 5) Little Cottonwood Canyon in Utah will be utilised. The latitudinal and longitudinal extents of the study area are mentioned in Table 1. NASA's SnowEx campaign has been successfully used in the past for estimating snow depth values (Currier et al., 2019; Marshall et al., 2021). The uncertainties in this dataset were not explored; thus, the analysis proceeded under the assumption that this data is accurate and reliable. These images were used as reference datasets in this study. SAR images from Sentinel-1, SAOCOM, and UAVSAR, which spatially overlap with this reference dataset, were acquired.

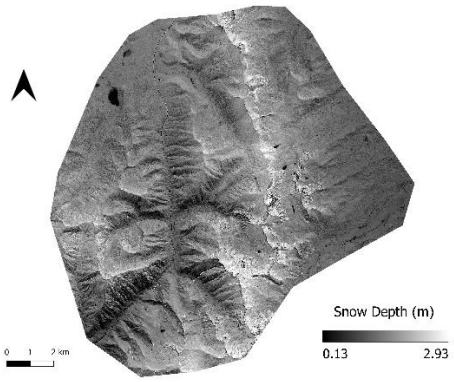

(a) Basin Summit, Idaho

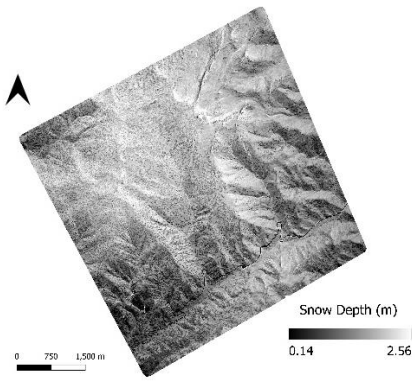

(b) Mores Creek, Idaho

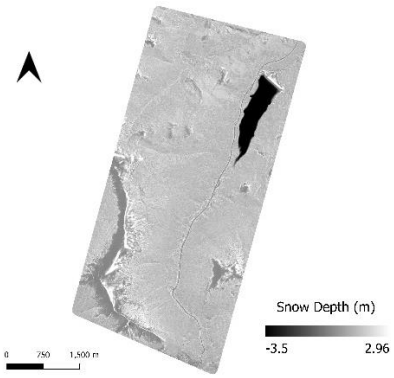

(c) Cameron Pass, Colorado

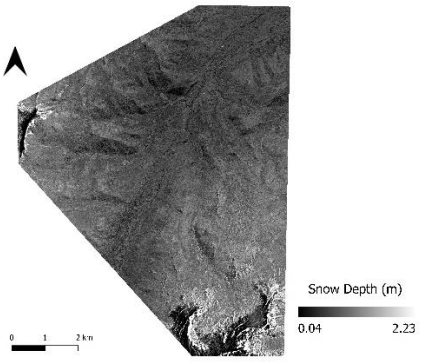

(d) Fraser, Colorado

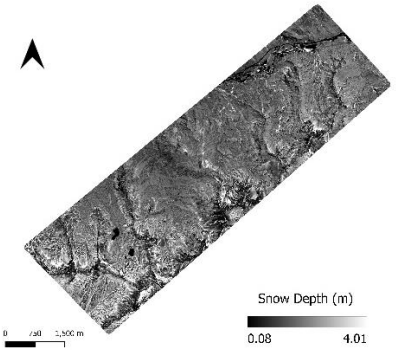

(e) Little Cottonwood Canyon, Utah

Figure 2: Snow depth images used in this study, visualised in greyscale for all research sites: (a) Basin Summit, Idaho, (b) Mores Creek, Idaho, (c) Cameron Pass, Colorado, (d) Fraser, Colorado, (e) Little Cottonwood Canyon, Utah

2.2.2. Sentinel-1

Sentinel-1, a SAR mission, was launched by the European Space Agency (ESA) in 2014. The constellations made by Sentinel-1A and Sentinel-1B are positioned at a distance of 180° in the polar orbit. Sentinel-1 comprises a C-band SAR sensor that operates at a frequency of 5.405 GHz and transmits data in both single (HH and VV) and dual polarised (HH+HV and VV+VH) modes. It offers two types of products while collecting data in four different acquisition modes. The Ground Range Detected (GRD) product only provides amplitude information. This research will explore the VV+VH dual-polarimetric (DP) Level-1 GRD high-resolution data from Interferometric Wide Swath (IW) acquisition mode, which covers a 250 km swath. In total 4 images for the entire region of interest were downloaded from ESA's Copernicus Open Access Hub. The ground range and azimuth resolution of the imagery correspond to 10 m by 10 m respectively. To ensure temporal consistency with the reference SnowEx Snow Depth dataset, Sentinel-1 images of the same time period are utilised. Figure 3 shows the Sentinel-1 images clipped according to the study area sites. Sentinel-1 data has been frequently used for SDE (Li et al., 2022; Lievens et al., 2022; Varade et al., 2020).

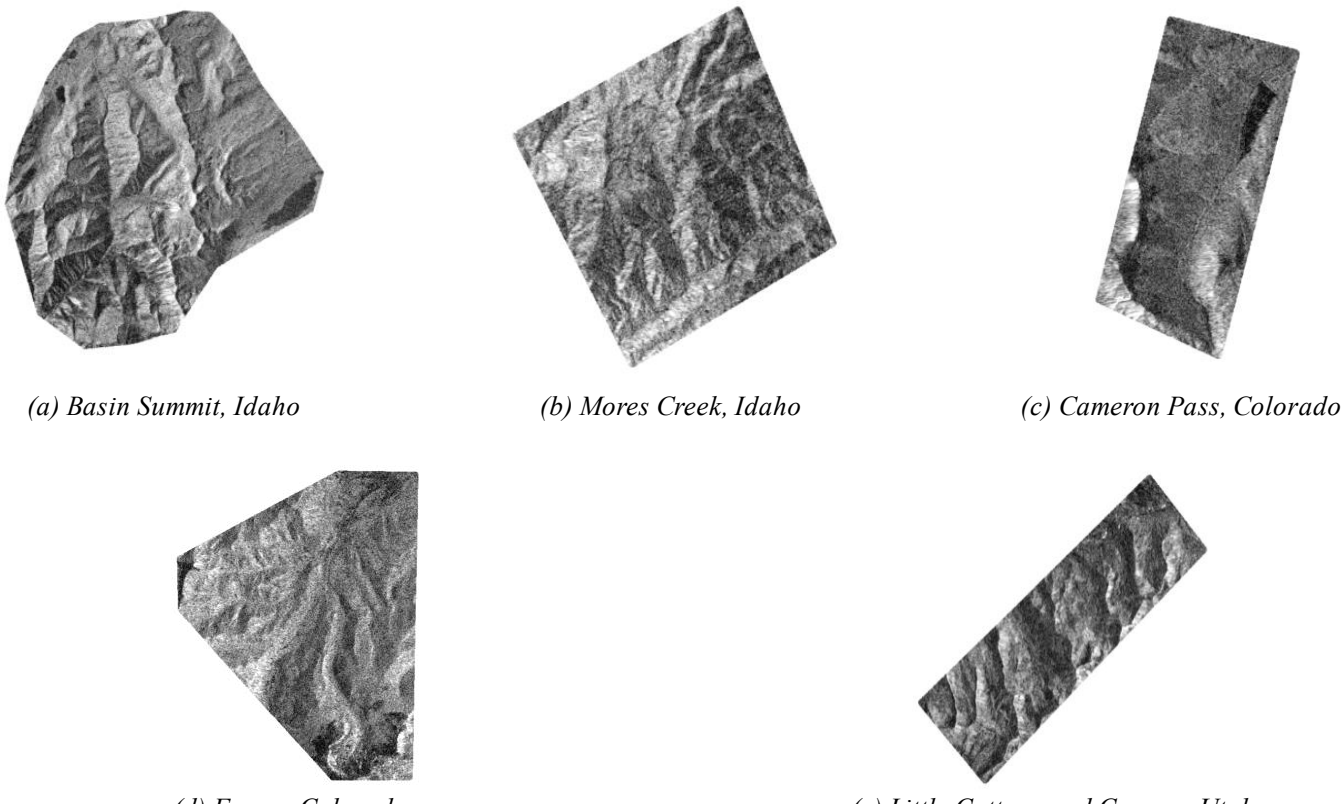

(a) Basin Summit, Idaho *(b) Mores Creek, Idaho* *(c) Cameron Pass, Colorado*

(d) Fraser, Colorado *(e) Little Cottonwood Canyon, Utah*

Figure 3: Sentinel-1 images used in this study, visualising the intensity of VH band (dB) in greyscale for all research sites: (a) Basin Summit, Idaho, (b) Mores Creek, Idaho, (c) Cameron Pass, Colorado, (d) Fraser, Colorado, (e) Little Cottonwood Canyon, Utah

2.2.3. UAVSAR

UAVSAR is built by the Jet Propulsion Laboratory (JPL). JPL is a NASA-funded research and development facility run by the California Institute of Technology (Caltech) (Hensley et al.,

2008). The radar, introduced by NASA in 2007, is intended for use on aeroplanes or UAVs (Rosen et al., 2006). Mounted on a NASA Gulfstream III aircraft, the UAVSAR platform operates in full-polarisation mode. It has a sensor frequency of 1.26 GHz and provides data in the L-band. For the NASA SnowEx program in 2020 and 2021, UAVSAR was tasked with conducting weekly to biweekly observations across 14 sites in the western United States from January to March (Hoppinen et al., 2024). The UAVSAR imagery, georeferenced and terrain corrected with the Shuttle Radar Topography Mission (SRTM) DEM, was publicly accessible through the UAVSAR Data Search portal provided by NASA (Fore et al., 2015; Rosen et al., 2006). The processing level for the data is GRD and provides amplitude information at a range and azimuth resolution of 1.8 m each. Four UAVSAR images spanning all the research sites that were collected in March 2021 (see Table 3 for dates) will be used for this study. Figure 4 shows the UAVSAR images clipped according to the study area sites. UAVSAR has been used for snow depth estimates in the past (Deeb et al., 2017; Palomaki & Sproles, 2023).

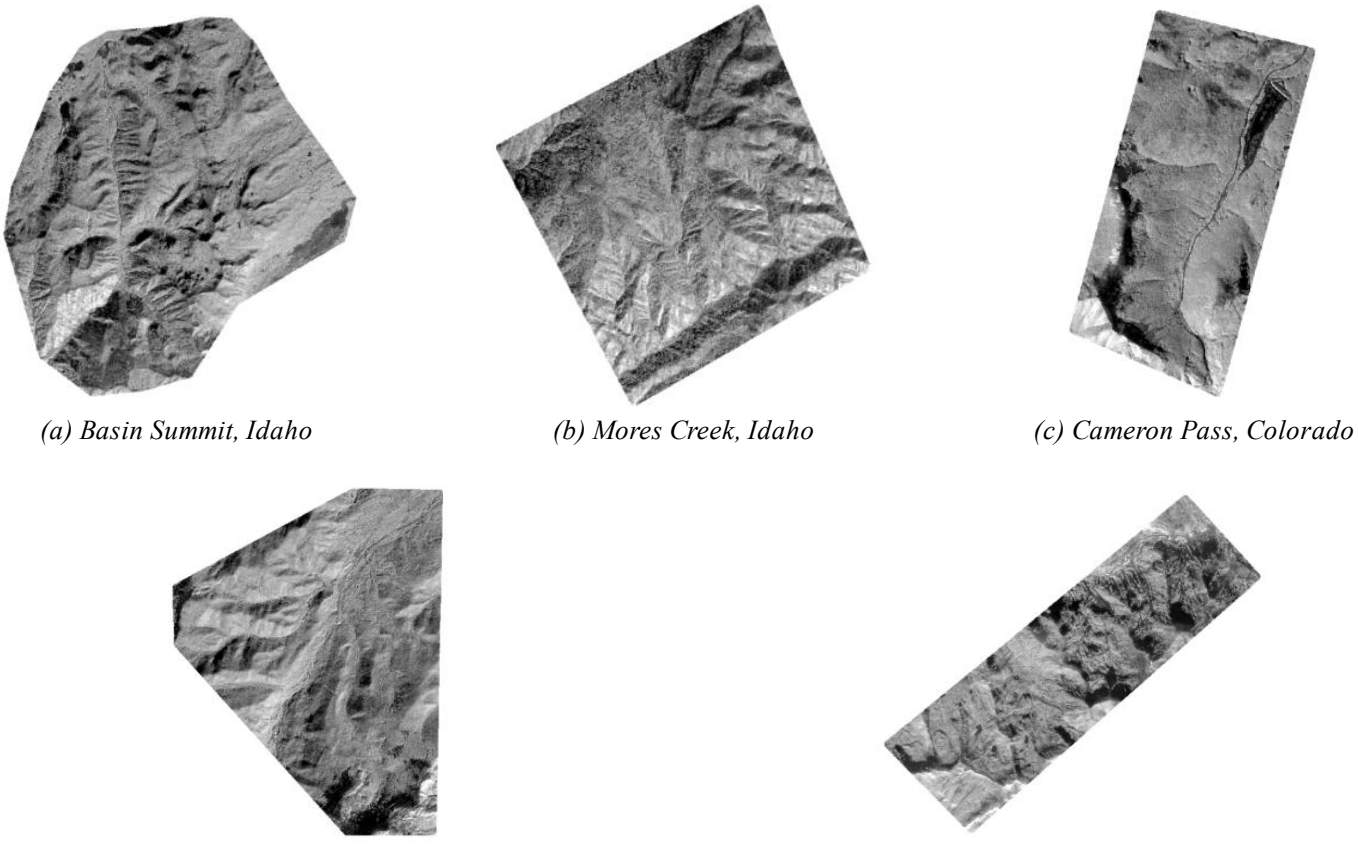

(a) Basin Summit, Idaho *(b) Mores Creek, Idaho* *(c) Cameron Pass, Colorado*

(d) Fraser, Colorado *(e) Little Cottonwood Canyon, Utah*

Figure 4: UAVSAR images used in this study, visualising the intensity of HH band (dB) in greyscale for all research sites: (a) Basin Summit, Idaho, (b) Mores Creek, Idaho, (c) Cameron Pass, Colorado, (d) Fraser, Colorado, (e) Little Cottonwood Canyon, Utah

2.2.4. SAOCOM

The SAOCOM constellation, which includes SAOCOM-1A and SAOCOM-1B, was launched in 2018 for microwave remote sensing purposes by Argentina's space agency, Comisión Nacional de ActividadesEspaciales (CONAE). It incorporates a SAR sensor that operates in the L-band (1,275 GHz,). DP and quad-polarimetric (QP) images providing complete coverage

of the study area sites will be used. The dataset consists of 3 images each of both polarisations acquired over different dates in March 2021 (see Table 3). Downloaded from the SAOCOM Catalog, the dataset's processing level is Level-1D, the product of which consists of amplitude information. L-1D Ground Terrain Corrected (GTC) data was chosen because it is already geometrically corrected, geocoded and georeferenced using topography. The acquisition mode of the instrument for this dataset is TOPSAR Narrow (TN) which corresponds to a ground range and azimuth resolution of 50 m and 50 m respectively. Figures 5 and 6 show the SAOCOM DP and QP images clipped according to the study area sites respectively.

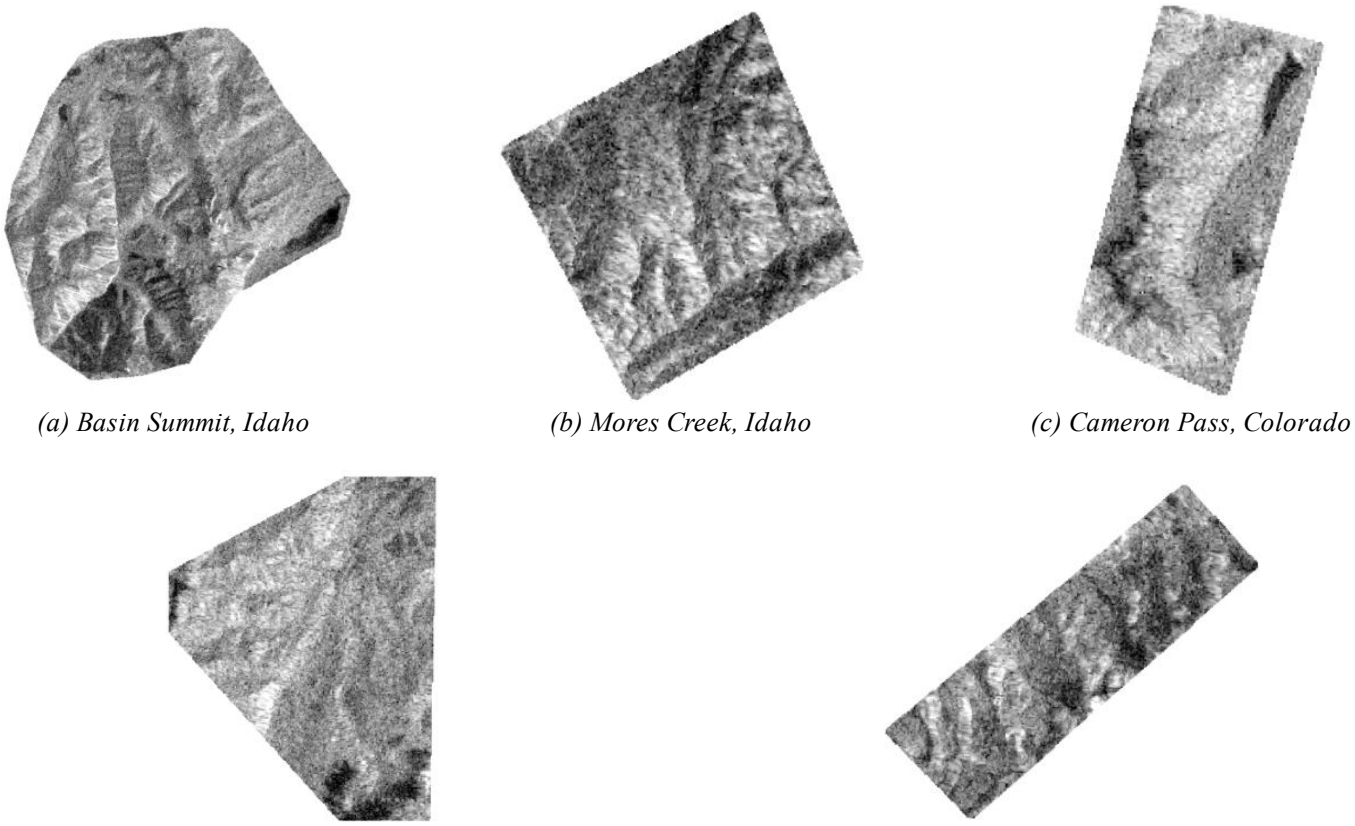

(a) Basin Summit, Idaho *(b) Mores Creek, Idaho* *(c) Cameron Pass, Colorado*

(d) Fraser, Colorado *(e) Little Cottonwood Canyon, Utah*

Figure 5: SAOCOM DP images used in this study, visualising the intensity of VH band (dB) in greyscale for all research sites: (a) Basin Summit, Idaho, (b) Mores Creek, Idaho, (c) Cameron Pass, Colorado, (d) Fraser, Colorado, (e) Little Cottonwood Canyon, Utah

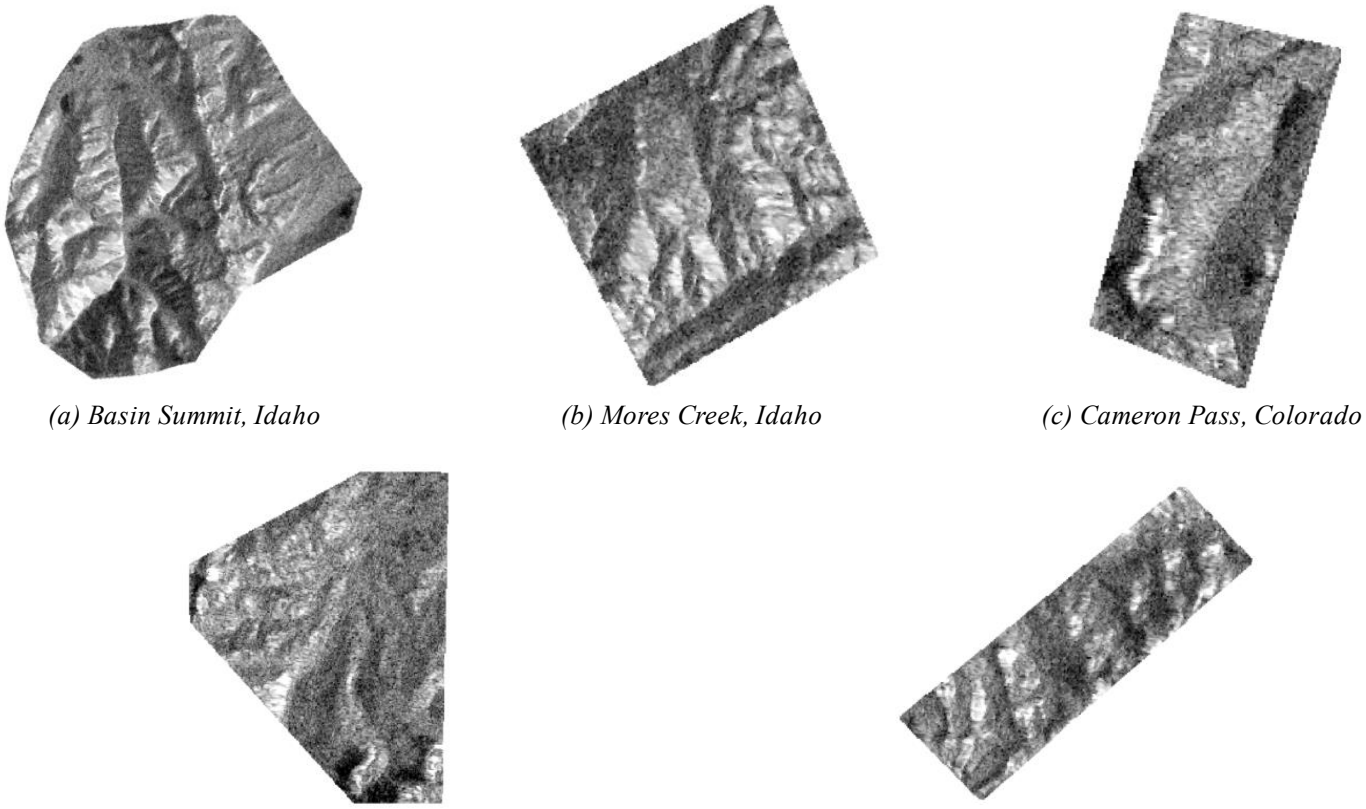

(a) Basin Summit, Idaho *(b) Mores Creek, Idaho* *(c) Cameron Pass, Colorado*

(d) Fraser, Colorado *(e) Little Cottonwood Canyon, Utah*

Figure 6: SAOCOM QP images used in this study, visualising the intensity of HH band (dB) in greyscale for all research sites: (a) Basin Summit, Idaho, (b) Mores Creek, Idaho, (c) Cameron Pass, Colorado, (d) Fraser, Colorado, (e) Little Cottonwood Canyon, Utah

Table 2: Summarised characteristics of SAR data sources

Characteristic	SENTINEL-1	SAOCOM DUAL	SAOCOM QUAD	UAVSAR
Band	C- band	L- band	L-band	L- band
Bandwidth	5.405 GHz	1.275 GHz	1.275 GHz	1.257 GHz
Polarization	Dual-Polarimetric (VH, VV)	Dual-polarimetric (VH, VV)	Quad-polarimetric (HH, HV, VH, VV)	Quad-polarimetric (HH, HV, VH, VV)
Processing Level	Ground Range Detected (GRD)	Ground Terrain Corrected (GTC)	Ground Terrain Corrected (GTC)	Ground Range Detected (GRD)
Ground Range and Azimuth Resolution	10 m * 10 m	50 m * 50 m	50 m * 50 m	1.8 m * 1.8 m
Instrument Acquisition Mode	Interferometric Wide Swath (IW)	TopSAR Narrow	TopSAR Narrow	PolSAR
Swath width	250 km	>150 km	>108 km	16 km
Wavelength	5.55 cm	23.51 cm	23.51 cm	23.79 cm

Table 3: Acquisition dates for all dataset

Study Area / Dataset	Fraser, Colorado	Cameron Pass, Colorado	Little Cottonwood Canyon, Utah	Basin Summit, Idaho	Mores Creek, Idaho
NASA SnowEx Snow Depth (reference data)	19th March 2021	19th March 2021	18th March 2021	15th March 2021	15th March 2021
Sentinel-1	30th March 2021	26th March 2021	21st March 2021	21st March 2021	21st March 2021
SAOCOM dual	6th March 2021	6th March 2021	18th March 2021	3rd March 2021	3rd March 2021
SAOCOM quad	6th March 2021	6th March 2021	18th March 2021	3rd March 2021	3rd March 2021
UAVSAR	22nd March 2021	16th March 2021	16th March 2021	16th March 2021	16th March 2021

2.3. Tools

Several tools and software were used in the research to handle various stages of study including data pre-processing, model generation, and evaluation. For the pre-processing of SAR imagery, the Sentinel Application Platform (SNAP) from the ESA and the ASF MapReady software from the Alaska Satellite Facility (ASF) were used. Creating training and testing samples and subsequently, model generation using random forest and quantitative assessments were performed in R programming language in RStudio. Furthermore, the predictions of the models were qualitatively evaluated by visualising the outputs in QGIS software.

CHAPTER 3

Methodology

3.1. Methodological Workflow

The flowchart in Figure 7 outlines the steps that will be executed to achieve this study's objectives and address the related research questions.

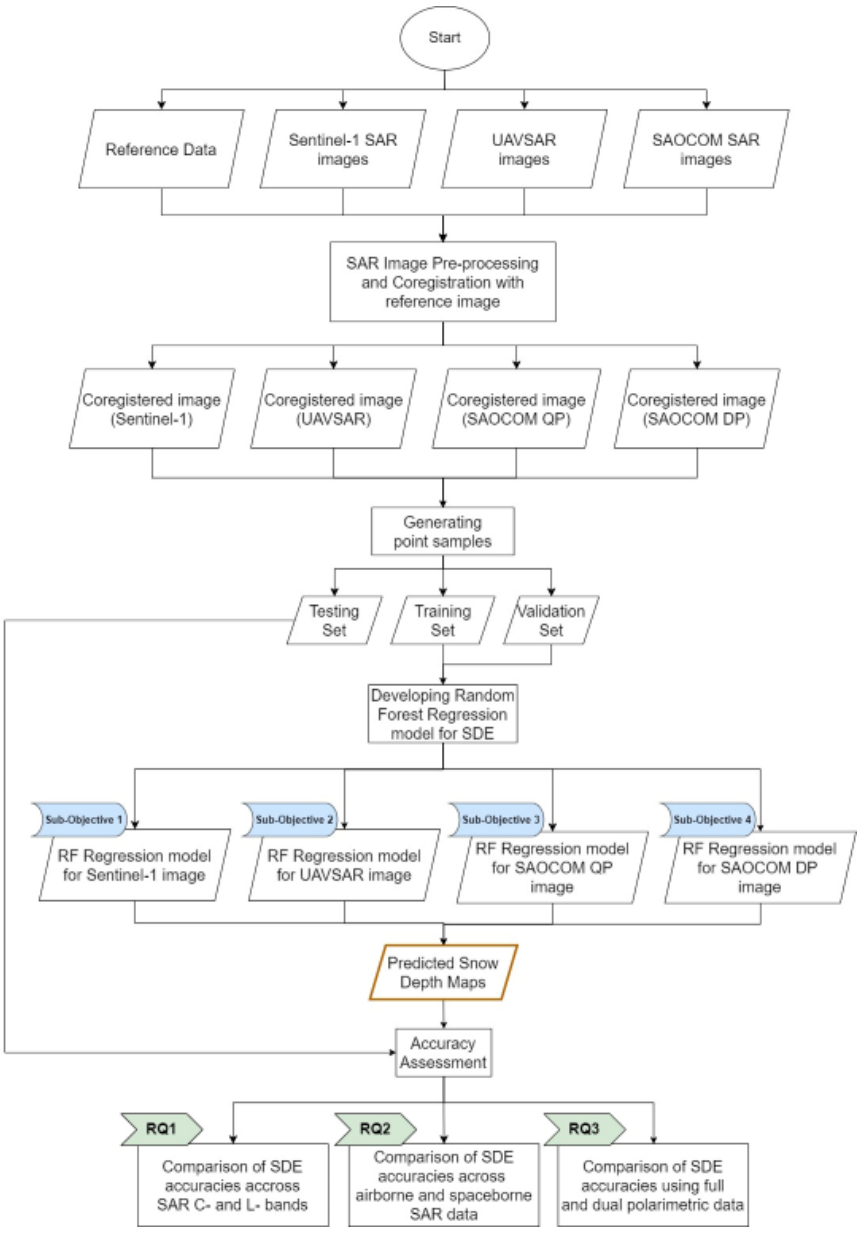

Figure 7: Methodological Workflow

3.2. Data Pre-processing

Despite their many benefits, SAR images have some inherent limits, which compromise the accuracy and quality of their data. Speckles and geometric distortions are a few of these drawbacks (Gabriel, 2002). Pre-processing methods must be used to overcome these restrictions and improve the accuracy and reliability of SAR-based SDE. The SNAP software, created by the European Space Agency (ESA), and ASF MapReady software created by ASF were used to perform the pre-processing of the SAR imagery. For missions like Sentinel-1, SAOCOM, and UAVSAR, these open-source software provide extensive SAR pre-processing capabilities.

3.2.1. Calibration

The first step was to perform radiometric calibration, which corrects and standardizes the pixel values or Digital Numbers (DN) to ensure they accurately represent the radar backscatter measurements from the Earth's surface. Additionally, with this process, one can transform the raw DN of the SAR image into physical units, namely sigma-nought (σ^0), gamma-nought (γ^0) and beta-nought (β^0) (El-Darymli et al., 2014). In all three of the parameters, brightness dependencies on incident angle have been widely noted. The dependency is most prominent in beta-nought, diminishing but still noticeable in sigma-nought, and even more so in gamma-nought (Atwood et al., 2012). Thus, gamma-nought (γ^0) was used for radiometric calibration because it helps remove the influence of incidence angle (Cheng et al., 2012). This was critical because the SAR datasets utilised in this study are acquired from a variety of sensor platforms, including both airborne and spaceborne sensors. These sensors have varying incidence angles. Using gamma-nought (γ^0) for radiometric calibration ensures more consistent and comparable backscatter values across all datasets. Thus, radiometric calibration was applied to all the SAR imageries of Sentinel-1 and SAOCOM-1 using SNAP software and the same was done for UAVSAR imageries using the ASF MapReady software.

3.2.2. Denoising

Speckle is a granular noise present in SAR images caused by interference and phase fluctuation (Singh & Shree, 2016). This inherent noise causes the salt and pepper effect, which was reduced by speckle filtering. Despeckling seeks to remove speckle noise while preserving the image's characteristics (Painam & Manikandan, 2023). The SAR images were filtered using the Refined Lee filter in SNAP. There is no option to change the kernel window size for this filter and its default is fixed to 7*7 in SNAP. The Refined Lee filter is chosen here for de-speckling as it excels in preserving details and features while effectively minimizing the blur effect (Yommy et al. 2015). Thus, the same speckle filtering process was applied to all SAR images in SNAP to remove noise and improve interpretability.

3.2.3. Geometric Correction

In this step, the SAR images were geocoded by projecting them to a target Coordinate Reference System (CRS) which gave each pixel a set of geographic coordinates based on the satellite's position. Ensuring consistency with the SnowEx snow depth images, the target CRS for the SAR images was set to EPSG:32611 – WGS 84 / UTM Zone 11N for the study areas

located in Idaho, EPSG:32612 – WGS 84 / UTM Zone 12N for the study areas in Utah, and EPSG:32613 – WGS 84 / UTM Zone 13N for the study areas in Colorado, respectively. Reprojecting the SAR dataset to a real-world geographic coordinate system is necessary to align it with the SnowEx snow depth dataset. Additionally, SAR images have some distortions caused by the side-looking geometry of radar (Filipponi, 2019). The main aim of geometric terrain correction was to somehow mitigate these distortions caused by terrain relief and bring the image's geometric representation as close to reality as feasible. The Range Doppler Terrain Correction option in SNAP uses a Digital Elevation Model (DEM) to adjust each pixel's location in order to correct geometric distortions brought on by topography, such as shadows and foreshortening (Filipponi, 2019). For all the SAR images of the study areas, we utilized the Copernicus 30m Global DEM, which is already available in SNAP. This DEM was chosen because its acquisition year 2021 closely aligns with the acquisition dates of the SAR data from March 2021. This temporal proximity aims to ensure greater accuracy while performing terrain correction as compared to older DEMs available in SNAP. Moreover, it gives accurate topographic information at a 30m spatial resolution which is suitable for terrain correction of SAR images (Ghannadi et al., 2023). Terrain correction wasn't applied to SAOCOM data because it is Level-1 GTC data which is already terrain-corrected. After this, the SAR images were clipped to the respective study area's extent in QGIS Software.

Figure 8 shows the first three preprocessing stages of a raw SAR image.

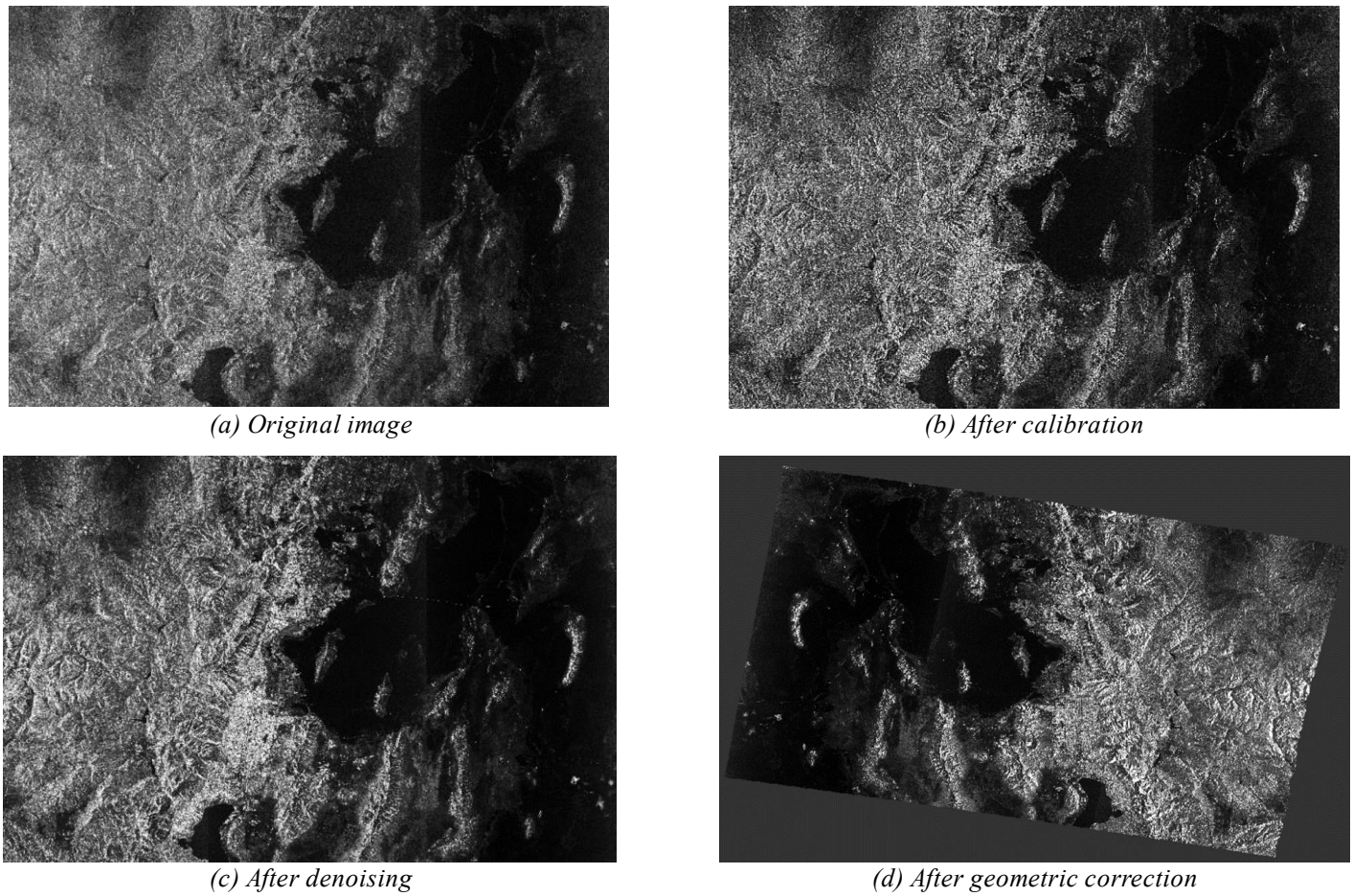

(a) Original image *(b) After calibration*

(c) After denoising *(d) After geometric correction*

Figure 8: The outcomes of a SAR image after applying the first four pre-processing stages, shown through the example of one of the Sentinel-1 images (visualising intensity of VH band) used during this study: (a) Original image, (b) Calibrated image, (c) Denoised image, (d) Geometrically corrected image

3.2.4. Georeferencing

SAR images provided by the SAOCOM satellite are inflicted with some geolocation errors where the pixels in the image can be displaced from their true geographic locations by a few metres (Mou et al., 2023). Upon visual inspection, it was noted that the SnowEx snow depth images weren't perfectly overlapping with the SAOCOM images. Thus, a manual georeferencing process was carried out using the Georeferencer tool in QGIS software. Ground Control Points (GCPs) were collected using the very high-resolution "Google Satellite" base map. A third-order Polynomial transformation was applied due to its ability to perform well in fitting GCPs accurately across the image (Das et al., 2018). For this transformation, the nearest neighbour resampling method was selected because it preserves the original pixel values (SAR backscatter), which is critical for this study. Finally, the georeferenced images of SAOCOM data, with their mean errors between 1.14 m to 1.61 m, were utilised for the subsequent pre-processing steps.

3.2.5. Conversion to Decibels (dB)

Radar sensors have high radiometric resolution due to which the range of the measured backscatter values is large. Thus, the unitless backscatter coefficient was transformed to dB in SNAP using a logarithmic transformation (see Equation 1). This normalises the data and can assist the machine learning models to learn more effectively.

$$Intensity\ (dB) = 10 * \log_{10}(Intensity) \quad (1)$$

3.2.6. Resampling of SnowEx snow depth data

To maintain consistency and alignment between the SAR imagery and the reference snow depth data, the reference data images were resampled to match the spatial resolutions of the respective SAR images. Specifically, the SnowEx snow depth rasters were resampled to a pixel spacing of 10 m *10 m for Sentinel-1, 50 m * 50 m for SAOCOM-1, and 1.8 m * 1.8 m for UAVSAR. This process allows for direct pixel-to-pixel correspondence between the SAR image and the SnowEx snow depth image. These resampled snow depth images were used for the subsequent steps.

3.2.7. Coregistration

In this step, coregistration was conducted to align SAR images with their corresponding resampled snow depth images using the SNAP software. The SAR image and resampled snow depth image were selected as input datasets for the coregistration process. The resampled snow depth image was designated as the master image, while the SAR image was designated as the slave image. Both images were stacked together to establish a single integrated reference geometry, ensuring their collocation and readiness for alignment. Coarse and fine registration techniques were employed to calculate cross-correlation between the SAR and snow depth images. Coarse registration initially aligned the images based on product geolocation, while fine registration refined the alignment by assessing image coherence at various window sizes. For warping, a third-degree polynomial transformation along with a cubic convolution interpolation was opted for, taking into account the complexity of the terrain in the study areas and to achieve precise alignment between the SAR and snow depth images. Before implementing the warping process, the distribution of Ground Control Points (GCPs) used in

the process was evaluated. Only GCPs with a root mean square error (RMSE) of less than 0.05 meters were utilized for warping, ensuring accurate coregistration at the sub-pixel level. This coregistration procedure ensures accurate spatial alignment, enabling reliable analysis between snow depth and their corresponding SAR backscatter intensity.

3.3. Developing a machine-learning model

3.3.1. Data Preparation

The next step, after pre-processing, was to prepare the data for the machine learning model. This process was carried out for all datasets associated with all the study areas of this study in the R environment using RStudio. 3000 points were generated by using random stratified sampling, ensuring a balanced representation of the variations in snow depth. This was done by stratifying the snow depth image into four classes based on their quantiles. These points were used to extract corresponding snow depth and SAR backscatter values from the stacked (coregistered) image. The SnowEx snow depth images contained some pixels with negative values and the interpretation of these values could contain uncertainty. Thus, the sample set was further filtered by deleting any points where the snow depth value was less than zero. This was done to ensure that only reliable and meaningful snow depth values were considered in the analysis.

This refined sample set was split randomly into temporary (70%) and testing (30%) sets. While adding points to the testing set, a condition was set that only the points lying outside a 100m buffer of the points in the temporary set were added to the testing set. This was done to minimize the effect of spatial autocorrelation to some extent. The temporary set was further split randomly into training (70%) and validation (30%) sets. Thus, 49% of the initial sample set made up the training set, 21% made up the validation set, and the remaining 30% became the testing set. By splitting the data in this way, the model was trained on one subset, validated on another, and then tested on an independent subset to assess its performance. A manual trial-and-error approach was carried out (only for 1 study area) with varying amounts of sample points, ranging from 1000 to 6000 points, with a step size of 1000. The models were shown to yield the best results when 3000 sample points were used. While there is a possibility that larger sample sizes might improve the machine learning model's precision in estimating snow depth, the computing time skyrocketed, making it unfeasible. Consequently, generating 3000 points achieved a balance between model accuracy and computing efficiency.

3.3.2. Random Forest Regression

Random forest (RF) is an ensemble method that builds several independent trees as a regression and uses statistical values to provide results (Segal, 2004). Regression trees serve as base learners and are grown from several subsets of training data that are produced by bootstrapping (bagging) (Rodriguez-Galiano et al., 2015). The outcome is derived from an individual tree and subsequently combined with the average of the trees being used to determine the final result (Breiman, 2001). The ability to model complicated and nonlinear relationships, resistance to overfitting, and robustness to the noise in the data are some of the advantages that RF regression offers over other statistical modelling methods (Seo et al., 2018). RF does a random selection of training samples and variables for splitting at each tree node, resulting in a huge number of trees, which makes the model insensitive to the quality of training

data (Maxwell et al., 2018). In addition, the RF model is user-friendly and quick to train (Tyralis et al., 2019). It has been recommended that the RF regression approach be used in remote sensing because of its excellent predictive power (Breiman, 2001; Hultquist et al., 2014).

For this study, the randomForest R package was used for developing and implementing the RF regression model on RStudio. The model was trained using the training samples set, with SAR backscatter values as predictors and snow depth values as the response variable. There will be two possible predictor variables (intensities of VH and VV band) in the case of DP SAR data and three possible predictor variables (intensities of HH band, HV band and VV band) in the case of QP SAR data.

3.3.3. Hyperparameter Tuning

Enhancing the model's performance typically involves tuning or setting several user-defined parameters, such as the number of trees in the ensemble (ntree), the number of random variables at each node (mtry) and the minimum size of terminal nodes (nodesize). A grid search was employed across a defined set of hyperparameters. This grid encompassed various values for ntree, mtry, and nodesize. Each combination of these parameters was used to train an RF regression model, which was subsequently evaluated. The performance of these models was measured through Root Mean Square Error (RMSE) and Mean Absolute Error (MAE). The model configuration that achieved the lowest RMSE and MAE values with the validation set provided the optimal combination of hyperparameter values. Finally, these parameters were employed to train the model with the training set, which was then used to predict snow depth values across the entire SAR image.

3.3.4. Accuracy Assessment

The testing set was utilised for the accuracy assessment to reveal how effectively the tuned model performs with unseen data. The performance of the models was assessed in a quantitative manner using the MAE (see Equation 2) and RMSE (see Equation 3). The MAE, also referred to as Mean Absolute Deviation, calculates the average of the absolute differences between observed and predicted values. MAE offers a straightforward interpretation of prediction accuracy by indicating the average size of the errors without considering their direction. The RMSE, also known as Root Mean Squared Deviation, is the square root of the mean of the squared errors. Essentially, RMSE represents the standard deviation of the prediction errors and indicates how closely the predicted values align with the observed data points. It is a commonly used accuracy metric (Karl, 2010; Spadavecchia & Williams, 2009). RMSE is sensitive to outliers and penalizes larger errors more heavily, while MAE treats all errors equally, providing a balanced perspective on overall prediction accuracy. Thus, the MAE and RMSE were computed for every model using the testing set. These methods have been recommended to assess the performance of the regression model (Adnan et al., 2017).

$$MAE = \frac{1}{N}\sum_{i=1}^{N} |SD_a - SD_p| \quad (2)$$

$$RMSE = \sqrt{\frac{1}{N}\sum_{i=1}^{N}\left(SD_a - SD_p\right)^2} \quad (3)$$

Where N is the total number of observations, SD_a is the actual snow depth and SD_p is the predicted snow depth.

Along with the assessment using MAE and RMSE, p-values were computed to evaluate the statistical significance of the relationship between the predictor and the response variable. It helps determine whether the RF regression model's findings are due to random chance or if there is a statistically significant relationship between the variables. It facilitates formal hypothesis testing, allowing the testing of the alternative hypothesis (H_1) against the null hypothesis (H_0) (De Leeuw et al., 2006).

H_0 – There is no statistically significant relation between the SAR backscatter values and the snow depth values.
H_1- There is a statistically significant relation between the SAR backscatter values and the snow depth values.

A low p-value ($p < 0.05$) indicates that the null hypothesis was rejected, indicating a statistically significant relationship between the predictors and the response variable. On the other hand, a higher p-value ($p \geq 0.05$) indicates weak evidence against the null hypothesis, implying that the observed relationship may be the result of chance.

3.3.5. Assessment of Spatial Generalization

To assess the model's spatial generalization ability, the training samples from four study areas (Mores Creek, Fraser, Cameron Pass, and Little Cottonwood Canyon) were combined and used to test the model on an independent, spatially disjoint study area (Basin Summit). This was done for all four SAR datasets and the same methodological workflow was followed as mentioned before. The RF regression model was trained using the combined training dataset with SAR backscatter values as predictors and snow depth as the response variable. The accuracy assessment was done utilizing the same testing set used previously for assessing the model performance over the same study area. The performance metrics (RMSE and MAE) of this new model with combined training data were compared with the model trained on the area's own training data.

CHAPTER 4

Experimental Results and Discussion

4.1. Results from model optimization analysis

4.1.1. Sensitivity of the model to training sample size

An investigation was done to examine how varying sample sizes affect the accuracy and computational efficiency of an RF regression model when predicting snow depth values from SAR backscatter values. The findings revealed that the RMSE and MAE values decreased as more sampling points were added to the training set, indicating an improved predictive capability and fewer errors in snow depth measurement. The time went up from 156.25 seconds for 1000 sampling points to 696.08 seconds for 3000 sampling points. Notably, the RMSE dropped from 0.61 m for 1000 sample points to 0.41 m for 3000 sample points, indicating a significant improvement in model precision. However, beyond 3000 samples, the improvements were minimal, and the computational time increased largely without significant improvements in accuracy. The RMSE and MAE values obtained with bigger sample sizes (4000, 5000 and 6000) were comparable to that of 3000; however, the processing time increased substantially, often doubling or tripling at these larger sample sizes. These results indicated that a sample size of 3000 points was optimal because the model execution time was 2x faster.

One aspect of the procedure carried out for this investigation is the random selection of sample points for each dataset size, which could possibly have an impact on the RMSE and MAE variations. Each set of points was selected randomly, possibly leading to variability in the features included in the training sample set. This suggests that while 3000 sample points appeared to be optimal, different randomly selected subsets of the same sample size could've produced different results. While iterating through different sample sizes, future research could also explore multiple iterations of sample selection (within the same sample size) to identify the most representative subset in each sample size and ensure more reliable conclusions. Generally, large training datasets result in higher accuracy for "data-hungry" machine learning models like RF regression (Domingos, 2012). Thus, this choice of using 3000 training samples for this study strikes a balance between model accuracy and computational time. Future studies could use cloud-based computing platforms such as the Geospatial Computing Platform (GCP) provided by the Center of Expertise on Big Geodata Science (CRIB) for the implementations of such models with large sample sizes in lesser runtime.

4.1.2. Checking for overfitting

Table 4 shows the RMSE and MAE values for training and validating dataset. All models show evidence of some extent of overfitting, as demonstrated by the slightly higher validation RMSE and MAE values compared to their respective training RMSE and MAE values. Amongst all datasets, Sentinel-1 shows the most extensive overfitting in a few cases, with significant differences between training and validation metrics. For instance, in Fraser, the Sentinel-1

model has a training RMSE of 0.421 m and a validation RMSE of 0.477 m, indicative of a severe fall in performance. Similarly, in Cameron Pass, the training RMSE for Sentinel-1 is 1.008 m, whereas the validation RMSE is 1.021 m, suggesting a relatively higher extent of overfitting compared to models of other datasets. Models with SAOCOM DP and QP datasets showed minimal differences between training and validation RMSE and MAE values implying limited overfitting. However, the UAVSAR dataset consistently exhibited the least overfitting for all regions. In Basin Summit, Idaho, for example, the training RMSE is 0.410 m and the validation RMSE is 0.415 m, with MAE values of 0.321 m and 0.330 m respectively.

Table 4: Performance metrics for training and validation sets

Study Area	Dataset	Training RMSE	Validating RMSE	Training MAE	Validating MAE
Basin Summit, Idaho					
	SAOCOM DP	0.519	0.531	0. 372	0.384
`	Sentinel-1	0.511	0.522	0.356	0.367
	SAOCOM QP	0.483	0.489	0.331	0.354
	UAVSAR	0.410	0.415	0.321	0.330
Mores Creek, Idaho					
	SAOCOM DP	0.524	0.544	0.411	0.425
	Sentinel-1	0.512	0.529	0.402	0.398
	SAOCOM QP	0.477	0.489	0.388	0.397
	UAVSAR	0.421	0.423	0.350	0.357
Cameron Pass, Colorado					
	SAOCOM DP	1.012	1.033	0.509	0.520
	Sentinel-1	1.008	1.021	0.503	0.521
	SAOCOM QP	0.965	0.972	0.495	0.503
	UAVSAR	0.884	0.900	0.472	0.489
Fraser, Colorado					
	SAOCOM DP	0.356	0.364	0.232	0.241
	Sentinel-1	0.421	0.477	0.265	0.273
	SAOCOM QP	0.342	0.355	0.238	0.245
	UAVSAR	0.405	0.447	0.260	0.274
Little Cottonwood Canyon					
	SAOCOM DP	0.817	0.830	0.627	0.629
	Sentinel-1	0.803	0.819	0.593	0.604
	SAOCOM QP	0.735	0.771	0.585	0.590
	UAVSAR	0.705	0.727	0.559	0.561

Overfitting in all the models implies that these models fitted too closely to the training samples and failed to generalize well. There exists a possibility that overfitting is occurring due to an insufficient training dataset that lacks enough sample points to accurately represent the range of input data (Ha et al., 2018). Additionally, the presence of noise in the training data could've

led to overfitting. If the model's complexity is too high, it learns and gets trained on the noise along with the useful information in the training dataset. From the results, although all models show some aspects of overfitting, it is noteworthy that the differences are not significant in most cases, suggesting that the overfitting is not very severe. Sentinel-1, however, shows higher extents of overfitting than others which might happen due to its specific characteristics. Its high spatial resolution, while beneficial for capturing details, might have introduced local variations that don't generalise well to the independent data. Moreover, SAOCOM products due to their low spatial resolution don't capture small-scale variations as compared to Sentinel-1 data, thus leading to minimal overfitting. Conversely, UAVSAR with the highest spatial resolution is the least overfitted during model implementation. The exact reasoning for these patterns requires further investigation. Since the difference in RMSE and MAE in the validation set after hyperparameter tuning is only a few centimetres, overfitting is not severe and thus no action was taken. However, it is acknowledged that overfitting, even though minimal, is not ideal. Thus, future models can focus on utilising regularisation techniques to avoid overfitting (Ghojogh et al., 2019).

4.2. Results from RF regression analysis

The performance metrics established by using the testing set to assess the accuracy of the predicted maps generated by the RF regression models, including RMSE, MAE, and p-value are given in Table 5.

Table 5: RMSE, MAE and p-value achieved by assessing the models on the testing set

Study Area	Dataset	RMSE	MAE	p-value
Basin Summit, Idaho				
	SAOCOM DP	0.549	0.400	0.0042
	Sentinel-1	0.540	0.388	0.0009
	SAOCOM QP	0.502	0.360	0.0425
	UAVSAR	0.438	0.327	1.78×10^{-7}
Mores Creek, Idaho				
	SAOCOM DP	0.554	0.430	1.92×10^{-5}
	Sentinel-1	0.549	0.415	0.02388
	SAOCOM QP	0.492	0.406	8.90×10^{-6}
	UAVSAR	0.439	0.364	2.20×10^{-16}
Cameron Pass, Colorado				
	SAOCOM DP	1.038	0.527	3.11×10^{-6}
	Sentinel-1	1.029	0.523	0.00085
	SAOCOM QP	0.980	0.520	4.56×10^{-6}
	UAVSAR	0.907	0.487	2.20×10^{-16}
Fraser, Colorado				
	SAOCOM DP	0.449423	0.282026	0.6108
	Sentinel-1	0.460416	0.2935155	0.00078
	SAOCOM QP	0.40537	0.27818	0.0003

	UAVSAR	0.42468	0.2873148	0.6425
Little Cottonwood Canyon				
	SAOCOM DP	0.859	0.635	0.1556
	Sentinel-1	0.821	0.605	0.5059
	SAOCOM QP	0.788	0.610	0.1389
	UAVSAR	0.730	0.591	0.02464

A model with smaller RMSE and MAE values suggests better predictive accuracy. In Mores Creek, the lowest RMSE (0.42 m) and MAE (0.36 m) values were achieved using the UAVSAR dataset. Following UAVSAR, SAOCOM QP showed RMSE and MAE values of 0.49 m and 0.40 m, respectively. Sentinel-1 closely followed with an RMSE of 0.54 m and MAE of 0.41 m. SAOCOM DP dataset displayed the highest RMSE and MAE values of 0.55 m and 0.43 m, respectively. A similar trend is seen (see Figure 9 and Table 5) in Basin Summit, Cameron Pass, and Little Cottonwood Canyon where UAVSAR outperformed other datasets with the lowest RMSE and MAE, followed by SAOCOM QP, Sentinel-1, and SAOCOM DP. These values highlight the significant variability in the performance of different datasets. Moreover, most of these RF regression models achieved a p-value less than 0.05, indicating that their corresponding results are statistically significant and not due to random chance. Comparing across all study areas, the UAVSAR dataset in Basin Summit achieved the lowest overall RMSE (0.43 m) and MAE (0.32 m) in this study. The predictions of this model are reliable, which is supported by the model's small p-value of $1.78*10^{-7}$. On the other hand, the highest RMSE was observed with the SAOCOM DP dataset in Cameron Pass, which produced statistically significant outcomes with an RMSE of 1.03 m and an MAE of 0.52 m.

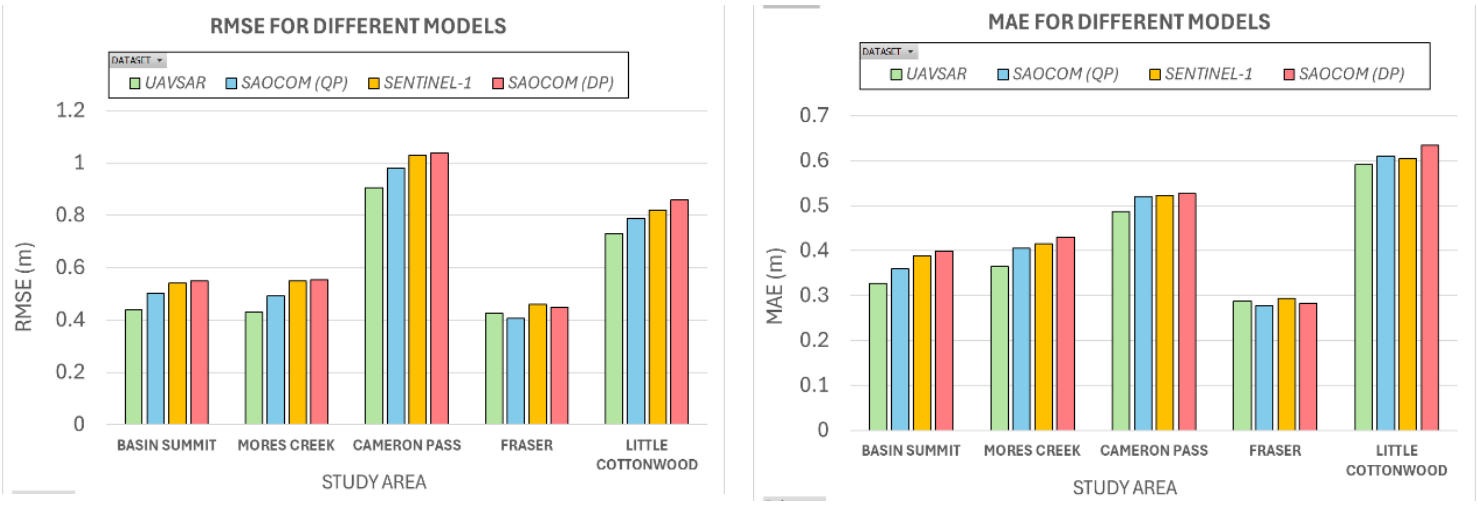

(a) RMSE *(b) MAE*

Figure 9: Performance metrics using the testing set for different models: (a) RMSE, (b) MAE

The quantitative results in Table 5 indicate that the datasets follow an order in terms of model performance and accuracy, with UAVSAR exhibiting the best results, followed by SAOCOM

QP data, Sentinel-1 and finally the SAOCOM DP data. The occurrence of this pattern is most likely to be a result of the specific characteristics of these datasets, such as its sensor's spatial resolution, polarisation configuration and frequency. UAVSAR's exceptional performance and accuracy in all the study areas are noteworthy. The lower RMSE and MAE values for UAVSAR across all study areas highlight its superiority over the other datasets used in this study for estimating snow depth. Having an airborne sensor platform, it has a very high spatial resolution that enables capturing finer details and identifying region-specific variations in the height of snow, leading to accurate predictions (Jones et al., 2013). It operates in the L-band, allowing for deeper penetration into the snowpack, which improves its ability to make accurate predictions about the depth of snow. Moreover, it employs full polarisation (HH, HV, VH, VV) which provides more comprehensive information about the snowpack as compared to dual polarization (Salma et al., 2022). The next best in line, spaceborne SAOCOM QP data has a much lower spatial resolution than UAVSAR, yet it compensates for the distance between sensor and snowpack through its deep-penetrating L-band data. Its fully polarimetric data, like UAVSAR, provides information in four channels (HH, HV, VH, VV). Sentinel-1 data, with its moderate spatial resolution of 10 m by 10 m, provided a better spatial resolution than SAOCOM QP data. However, it still resulted in higher RMSE and MAE values than SAOCOM QP data. This can be attributed to its dual polarization configuration that provides data only in two channels (VV and VH). Dual polarimetric data of Sentinel-1 offered lesser information to the model as compared to fully polarimetric SAOCOM QP and UAVSAR data. Moreover, Sentinel-1 operated in the C- band which has lesser penetration into the snowpack compared to the L-band, thus limiting its accuracy of snow depth measurements. The highest errors were observed in SAOCOM DP data. Coming from the same satellite, both SAOCOM DP and QP datasets have the same spatial resolution and frequency (L-band), yet the RMSE and MAE values are significantly higher in models of the SAOCOM DP dataset. Its dual-polarised data offering information in two channels provides lesser information to the model and limits the dataset's ability to estimate snow depth as accurately as the other fully polarised datasets. Interestingly, SAOCOM DP and Sentinel-1 achieved comparable results with very slight differences in their RMSE and MAE values. Although by a minor difference, Sentinel-1 has achieved more accurate predictions than SAOCOM DP. Both of them offer information in the same polarisation channels (VV and VH), however, SAOCOM DP operates in L- band, providing a deeper penetration into the snowpack but it is not enough to compensate for its low spatial resolution against the Sentinel-1, C- band, moderate resolution dataset.

In the Fraser region, the dataset accuracy trend deviated from the patterns seen in other research sites. Sentinel-1 had the highest RMSE of 0.46 m and MAE of 0.29 m. It also achieved a p-value less than 0.05 confirming that indeed the high values of RMSE and MAE are a result of meaningful interactions between the predictor and response variable. SAOCOM DP, with comparable values, achieved an RMSE of 0.44 m and MAE of 0.29 m. UAVSAR did not outperform the other datasets in this region, despite being the most accurate in the other study area sites. It yielded RMSE and MAE values of 0.42 m and 0.28 m, respectively. Interestingly, the SAOCOM QP dataset (RMSE: 0.40 m, MAE: 0.27 m) displayed comparatively lower error values, indicating improved performance in this specific study area. One possible reason for UAVSAR's higher error values could be that the training samples couldn't adequately represent the variability of snow depth in the Fraser region. The model might require a larger or more diverse set of samples to tackle such a problem. However, it is difficult to pinpoint the exact cause of UAVSAR's underperformance with surety without proper investigation. Furthermore, it is noteworthy that Little Cottonwood Canyon and Cameron Pass regions present significantly higher errors, representative of lesser predictive accuracy in these regions. For instance, in Cameron Pass, the UAVSAR dataset, despite being the most accurate among the datasets in

this region, recorded an RMSE of 0.9 m. and an MAE of 0.48 m which are higher than the corresponding values in other regions. Apart from model or training sample issues, such deviations from the usual trend might also be attributed to the local topography of these regions. SAR's side-looking geometry and the terrain distortions due to steep slopes or rugged terrains can tend to exhibit higher measurement errors (Zebker et al., 1997). However, further investigation is required to identify the underlying reasons for such deviations.

Figures 10 to 14 show the reference and predicted snow depth maps along with a difference map for all datasets across all study areas. The difference maps were generated by subtracting the predicted image from the reference image.

Through visual inspection of the maps, predicted maps from the UAVSAR dataset displayed the closest resemblance to the reference snow depth maps. The SAOCOM QP dataset showed more pronounced errors but still bears a fair amount of similarity to the reference snow depth values. The SAOCOM DP and Sentinel-1 datasets seem to show the largest discrepancies between the predicted and the observed snow depth values in the reference maps. It was also observed that the predicted snow depth maps generated by the models narrowed down the original range of snow depth values, indicating that the models failed to predict the full spectrum of snow depth values accurately in the study area. This failure to predict well is also confirmed by the high RMSE and MAE values of the models. The difference maps reveal areas where the model overestimated or underestimated the observed snow depth values. Overestimation is the case when the observed snow depth is minimal, yet the predicted values are higher. On the other hand, underestimation is the case when the observed snow depth is high, but the predicted value is low. All the models showed a tendency to slightly overestimate the snow depth values which were originally towards the lower end of the spectrum (close to 0) in the reference snow depth image. Similarly, underestimation was seen with snow depth values present originally in the higher end of the spectrum (close to the maximum snow depth of that region). This implies that the models showed a tendency to predict snow depths within a medium or middle range with respect to the reference data range, failing to predict the extremes. These difference maps also highlight where these errors are significantly higher. Upon visual inspection, it is evident that the highest errors (in both directions) are observed in areas where the snow depth values were either too high or too low, i.e., snow depth values were at the extreme ends of the reference data range.

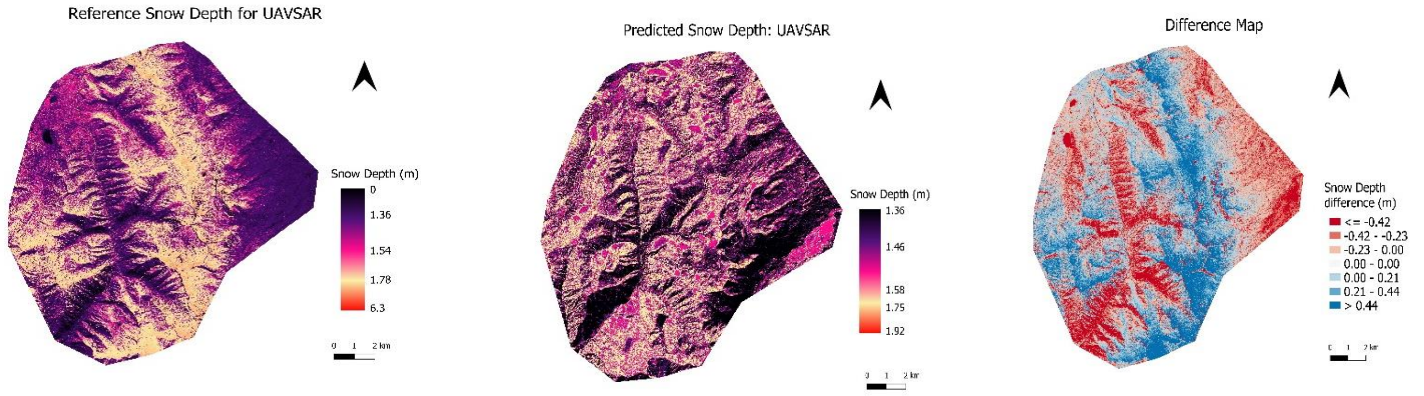

(a) UAVSAR

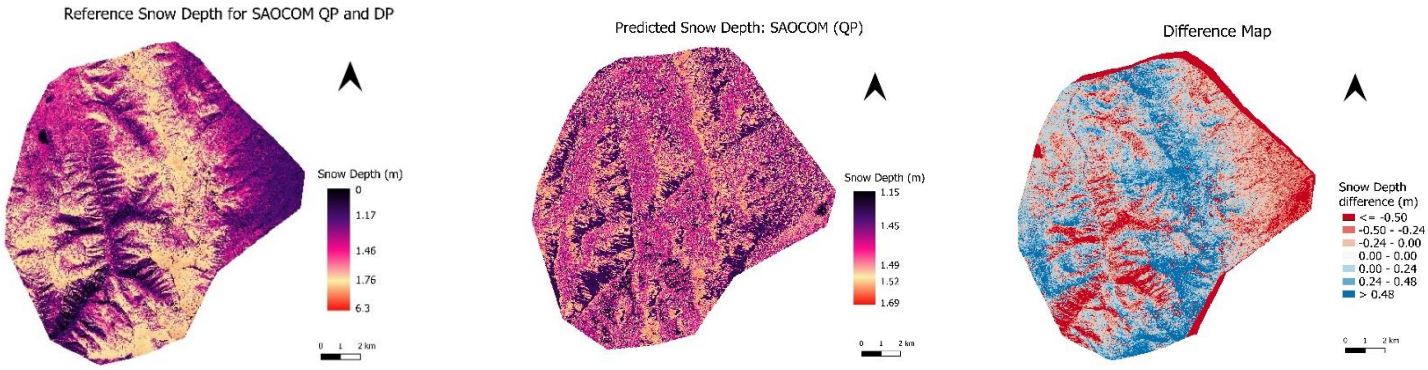

(b) SAOCOM QP

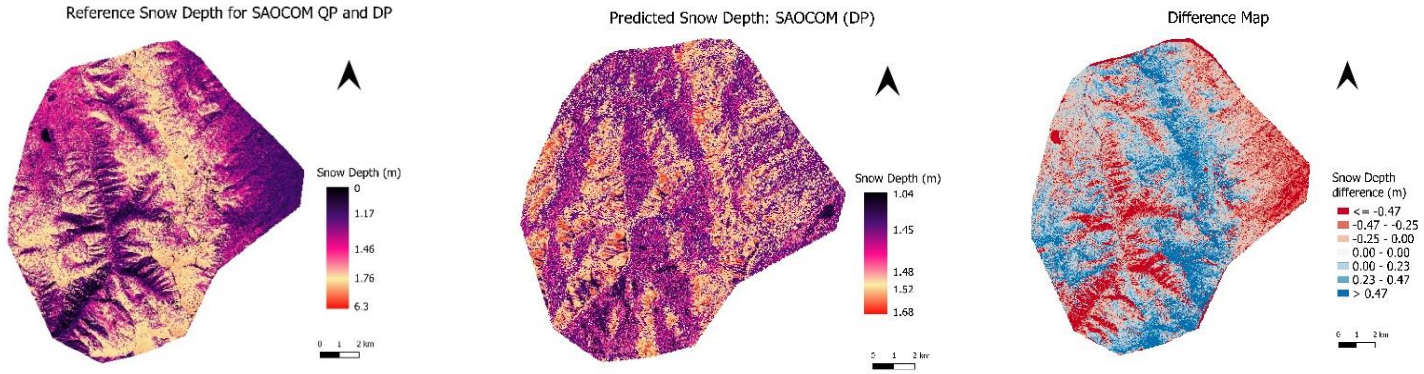

(c) SAOCOM DP

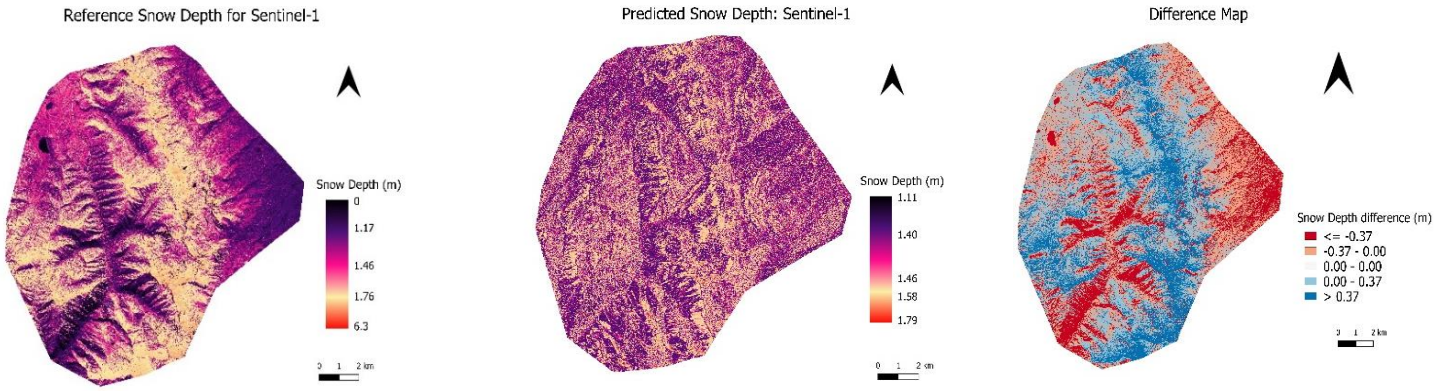

(d) SENTINEL-1

Figure 10: The reference (left), predicted (middle) and difference (right) snow depth maps for Basin Summit: (a) UAVSAR, (b) SAOCOM (QP), (c) SAOCOM (DP), (d) Sentinel-1

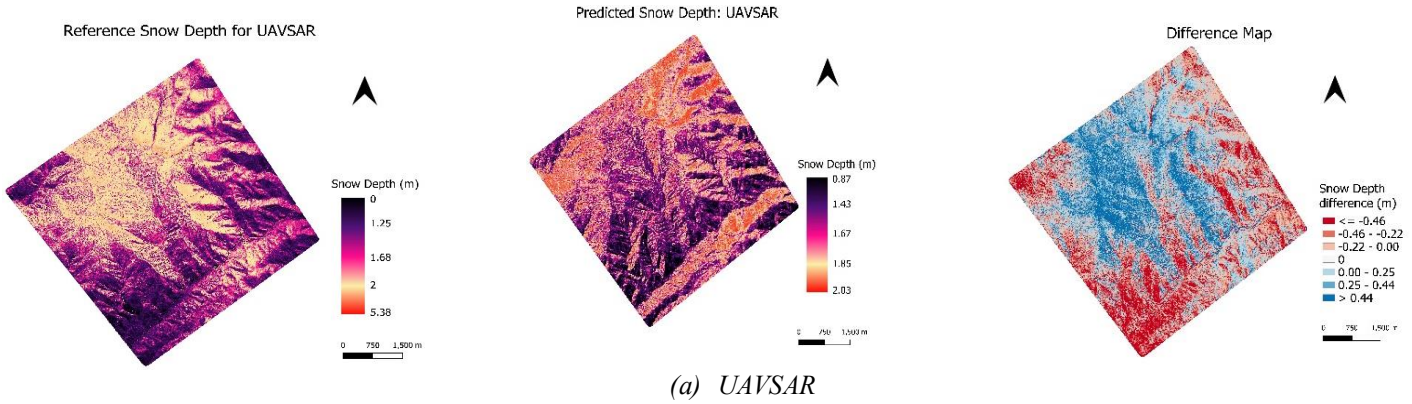

(a) UAVSAR

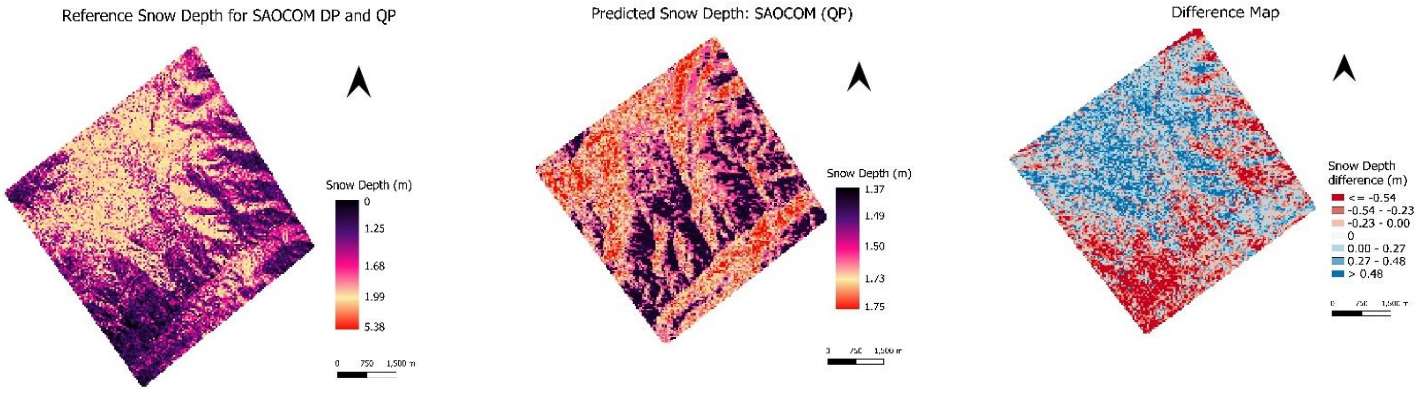

(b) SAOCOM QP

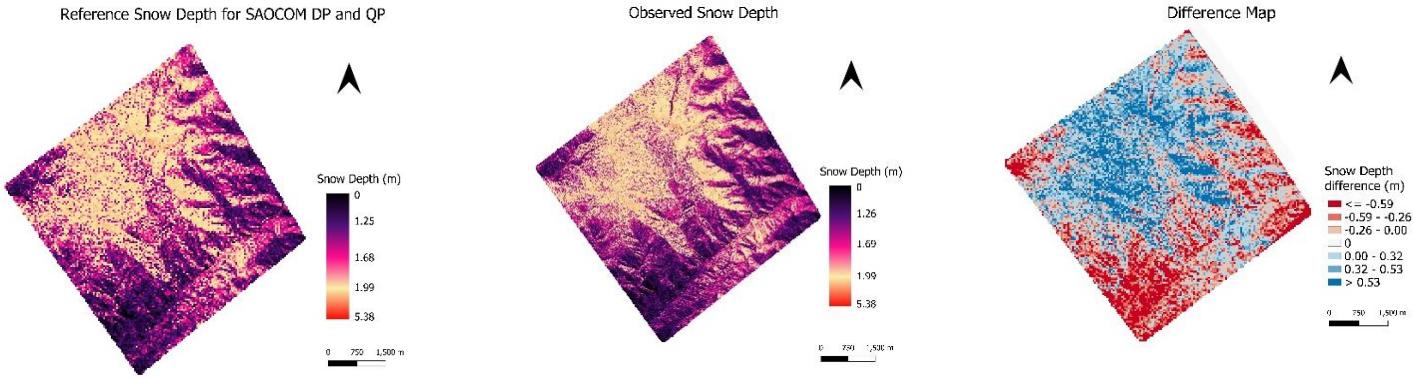

(c) SAOCOM DP

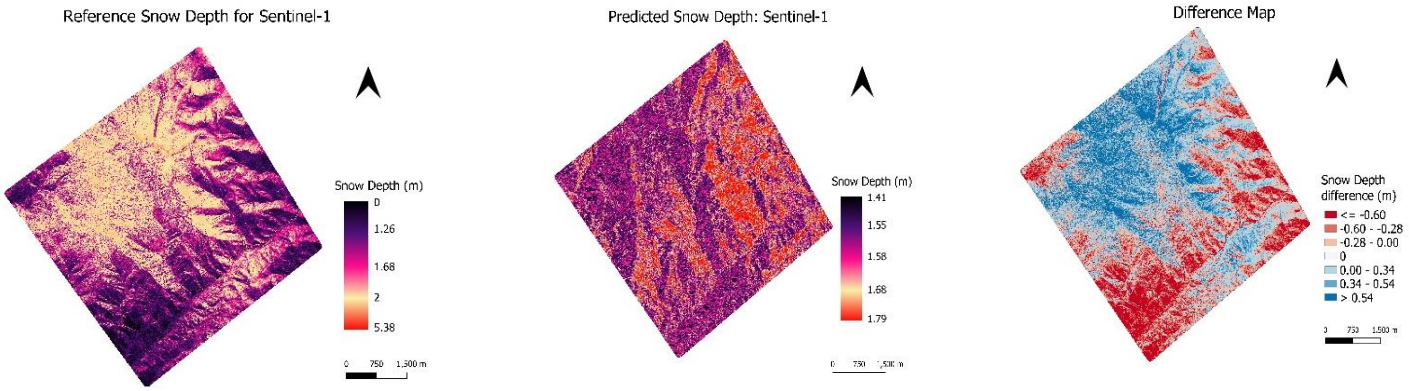

(d) SENTINEL-1

Figure 11: The reference (left), predicted (middle) and difference (right) snow depth maps for Mores Creek: (a) UAVSAR, (b) SAOCOM (QP), (c) SAOCOM (DP), (d) Sentinel-1.

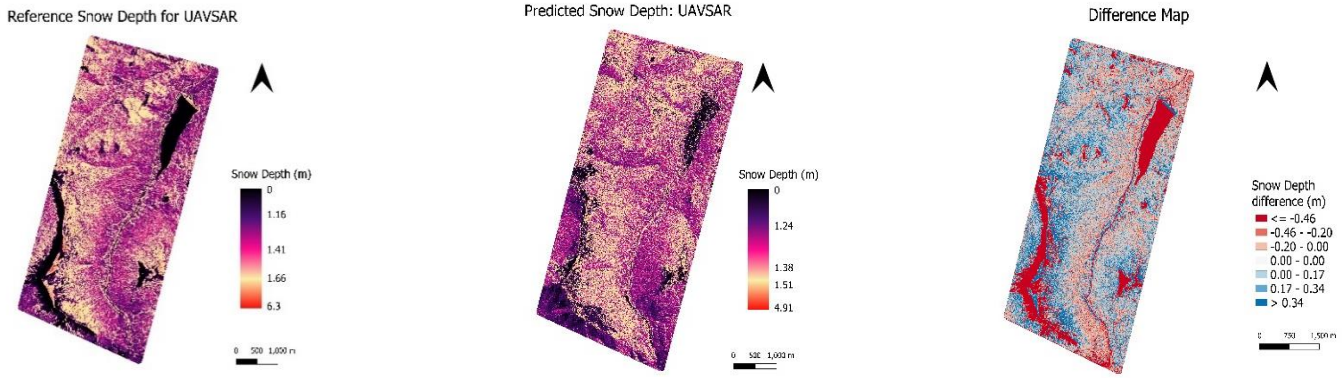

(a) UAVSAR

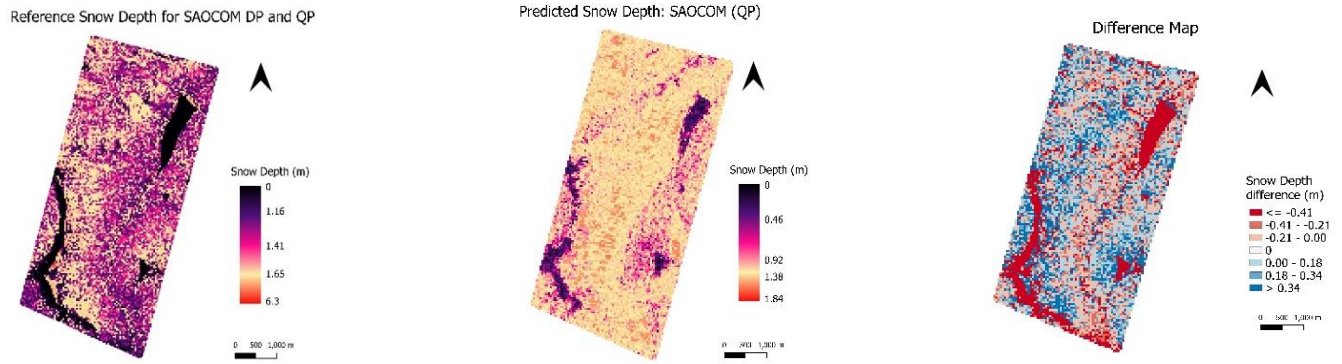

(b) SAOCOM QP

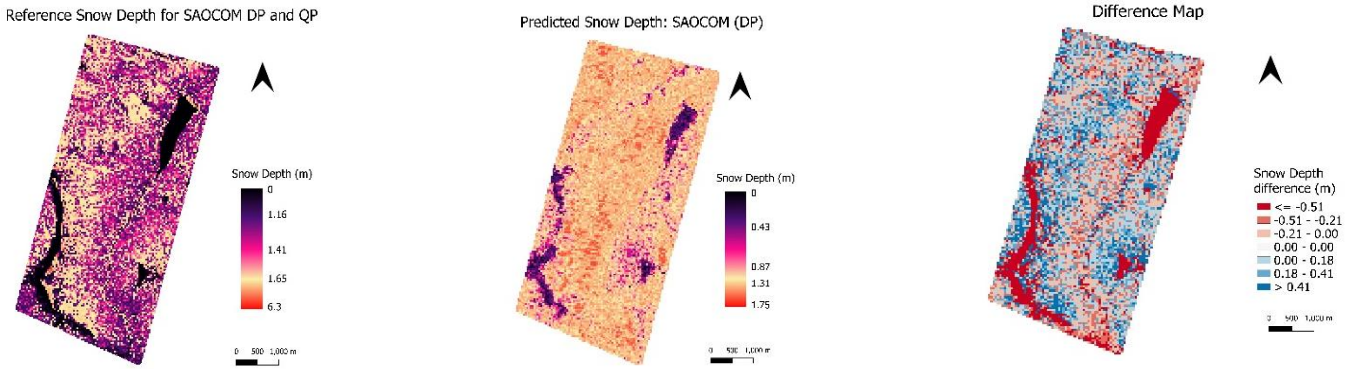

(c) SAOCOM DP

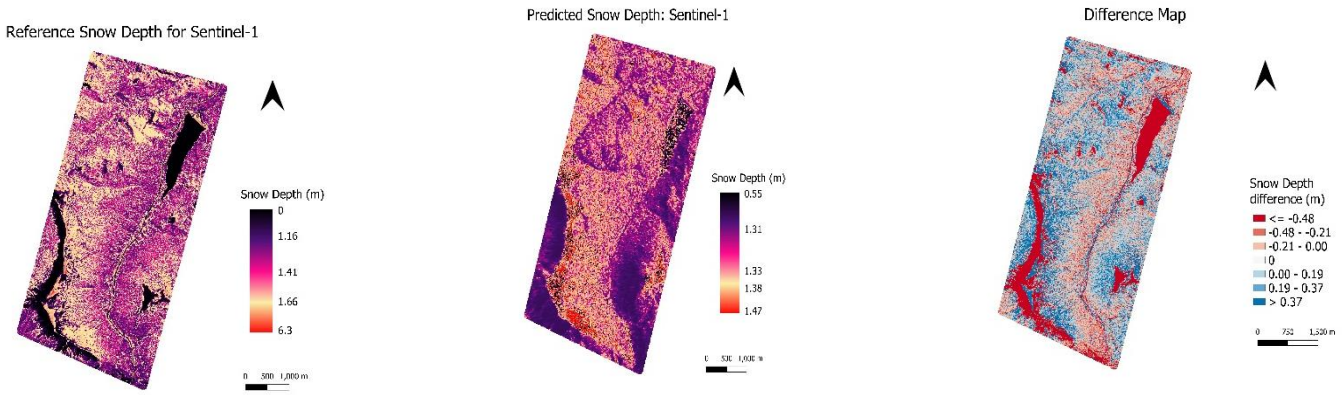

(d) SENTINEL-1

Figure 12: The reference (left), predicted (middle) and difference (right) snow depth maps for Cameron Pass: (a) UAVSAR, (b) SAOCOM (QP), (c) SAOCOM (DP), (d) Sentinel-1

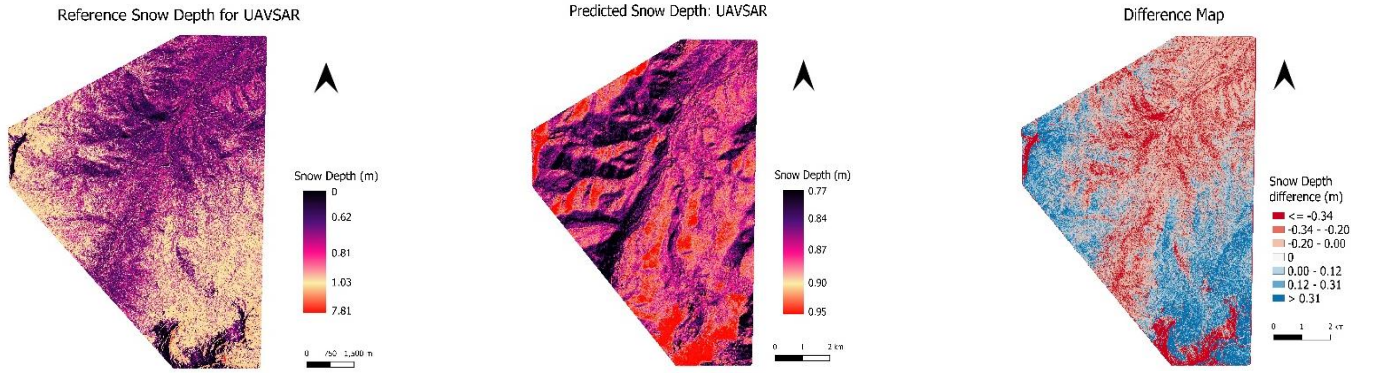

(a) UAVSAR

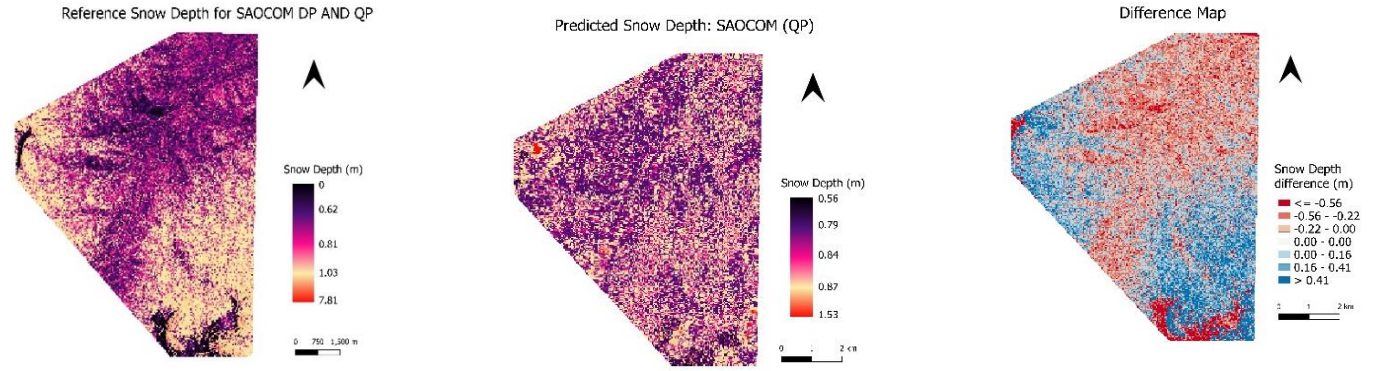

(b) SAOCOM QP

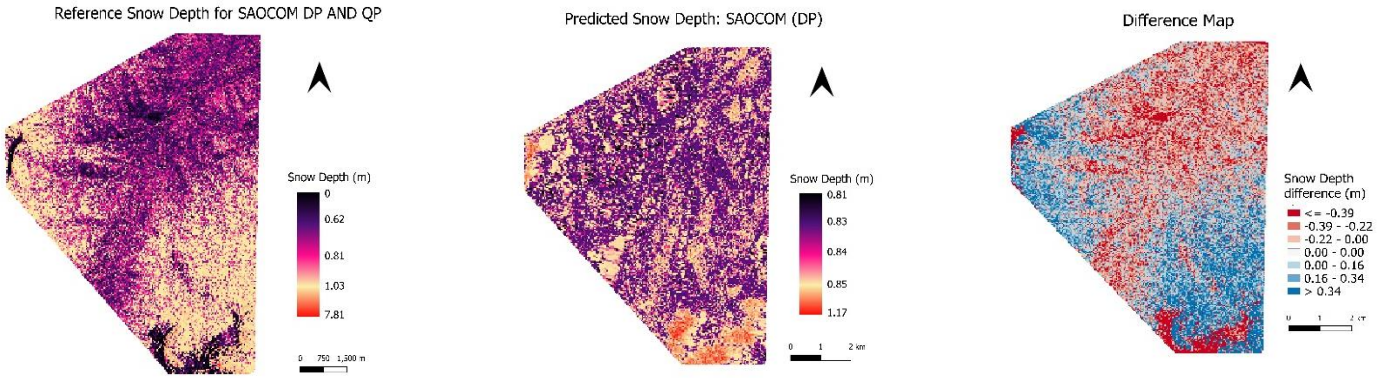

(c) SAOCOM DP

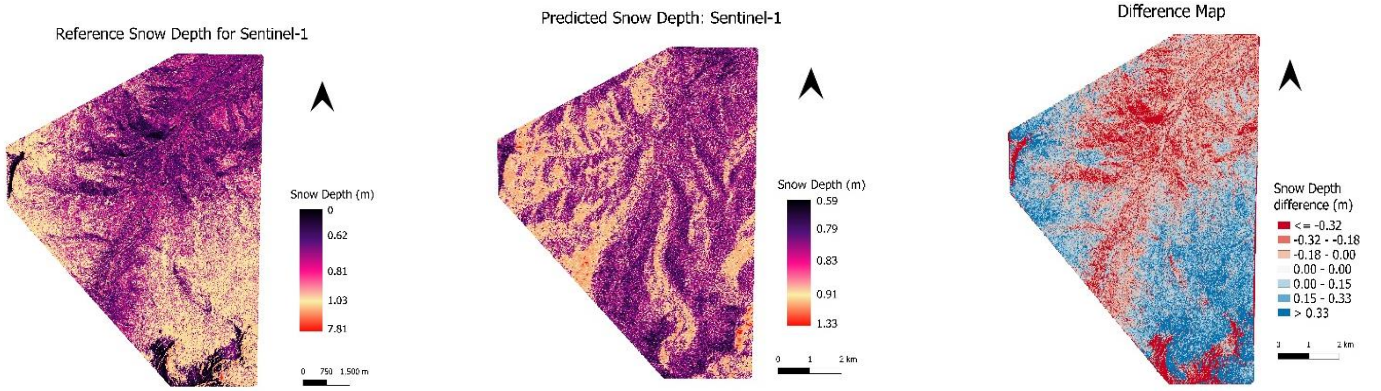

(d) SENTINEL-1

Figure 13: The reference (left), predicted (middle) and difference (right) snow depth maps for Fraser: (a) UAVSAR, (b) SAOCOM (QP), (c) SAOCOM (DP), (d) Sentinel-1

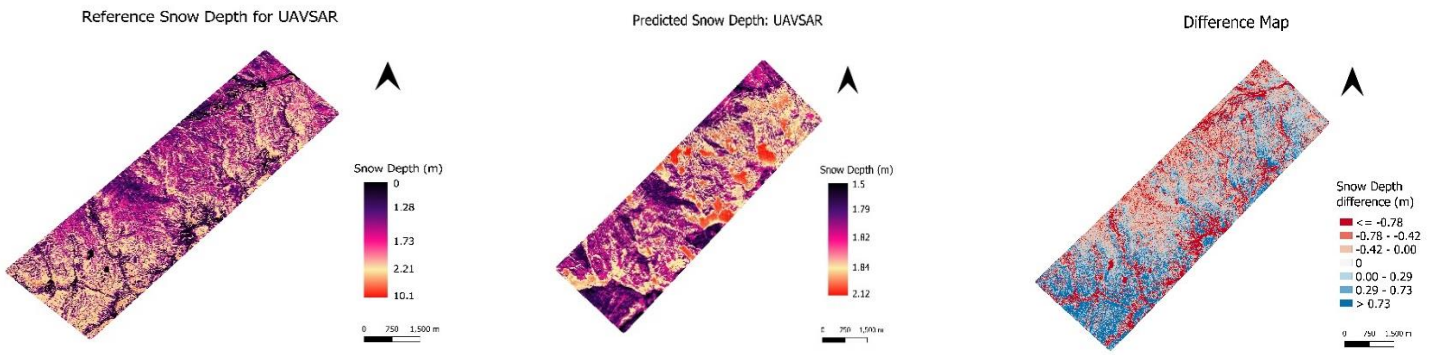

(a) UAVSAR

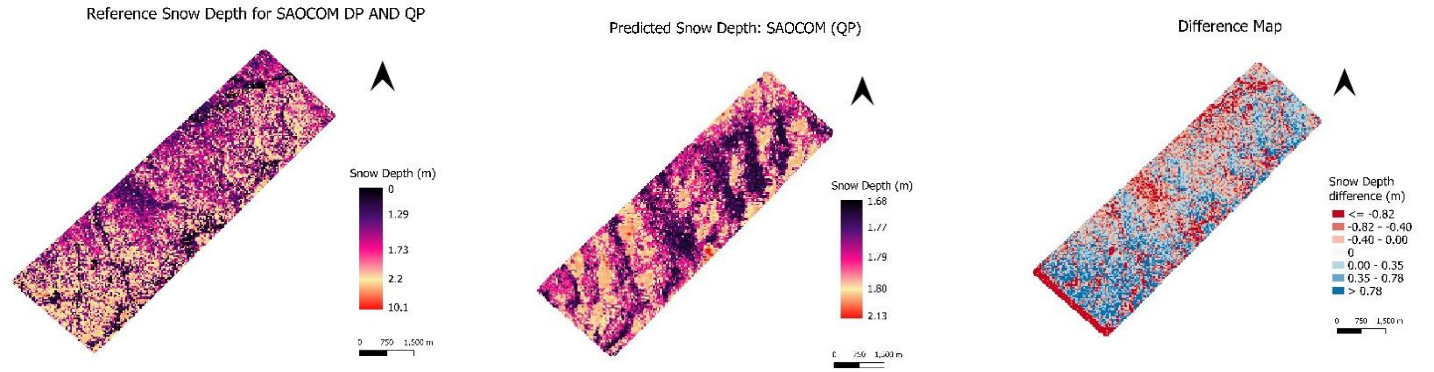

(b) SAOCOM QP

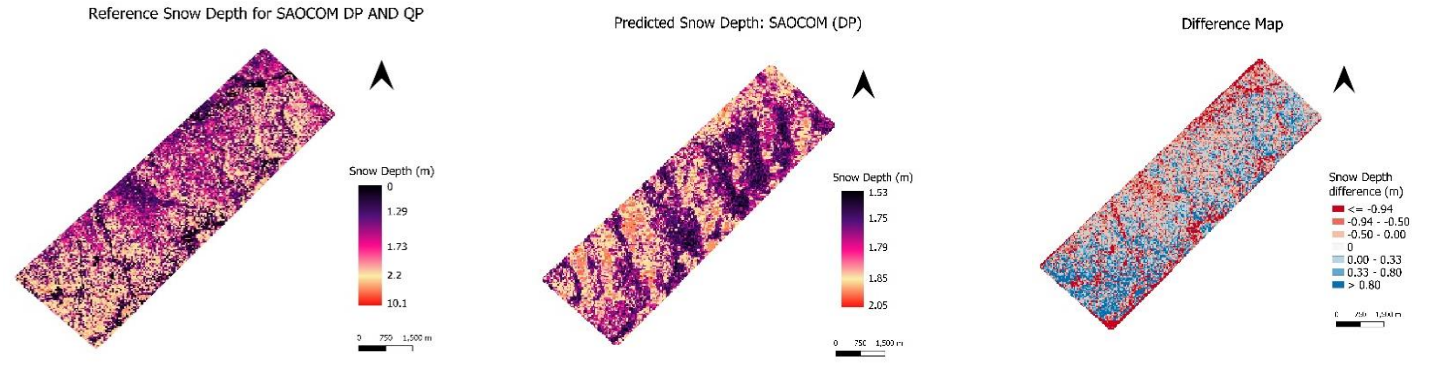

(c) SAOCOM DP

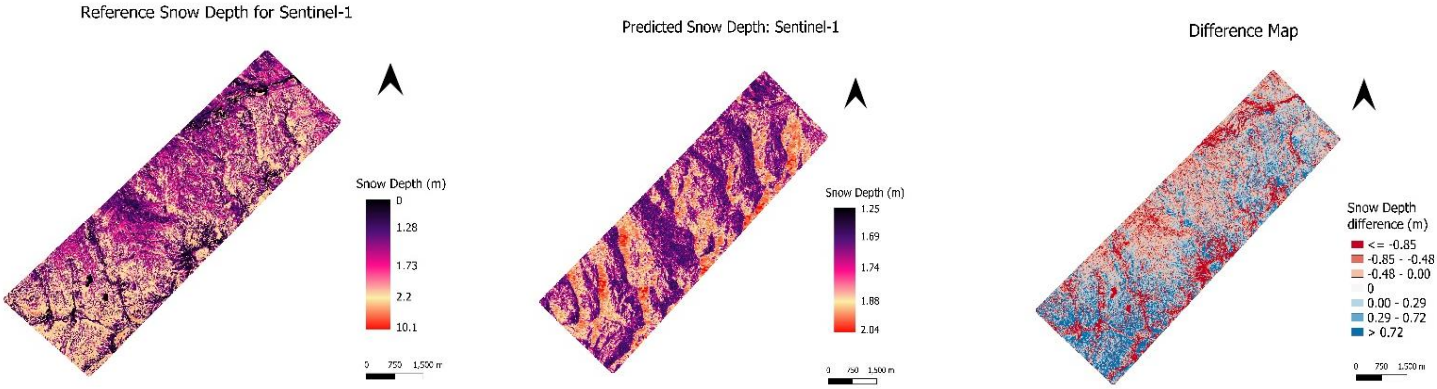

(d) SENTINEL-1

Figure 14: The reference (left), predicted (middle) and difference (right) snow depth maps for Little Cottonwood Canyon: (a) UAVSAR, (b) SAOCOM (QP), (c) SAOCOM (DP), (d) Sentinel-1

4.3. Results for model's generalisation ability

Table 6 shows the results obtained (combined RMSE, combined MAE) after training the model using combined training data from four study areas (Mores Creek, Fraser and Cameron Pass, Little Cottonwood Canyon) and testing it on a spatially disjoint study area (Basin Summit). The results revealed a slight increment in the RMSE and MAE values as compared to the results of the model trained using the area's own training samples.

Table 6: Model performance metrics (RMSE and MAE) for original and combined training sets

Dataset	RMSE (Old)	RMSE (Combined)	MAE (Old)	MAE (Combined)
SAOCOM DP	0.549	0.559	0.400	0.409
SENTINEL-1	0.540	0.550	0.388	0.374
SAOCOM QP	0.502	0.520	0.360	0.393
UAVSAR	0.438	0.515	0.327	0.383

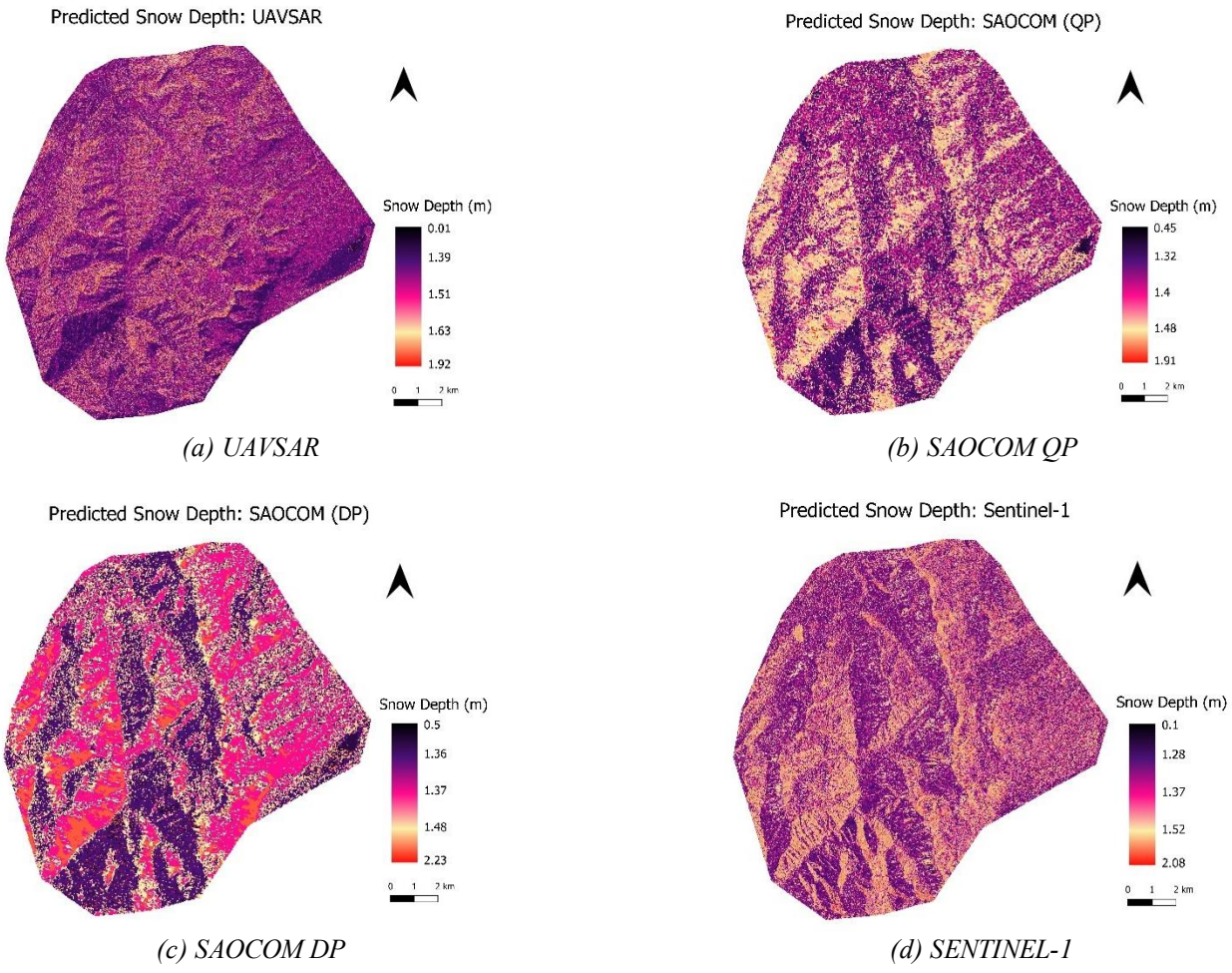

(a) UAVSAR *(b) SAOCOM QP*

(c) SAOCOM DP *(d) SENTINEL-1*

Figure 15: Predicted snow depth maps for the Basin Summit region, generated by training the models with training samples of spatially disjoint areas: (a) UAVSAR, (b) SAOCOM (QP), (c) SAOCOM (DP), (d) Sentinel-1

Though this investigation's outcome followed the previously observed trend in dataset performance —UAVSAR having the lowest RMSE and MAE, followed by SAOCOM QP, Sentinel-1, and SAOCOM DP— the performance of models decreased across all datasets. While the increment in RMSE and MAE values of SAOCOM DP, Sentinel-1 and SAOCOM QP is minimal, the UAVSAR dataset revealed a significant difference. The RMSE values only increased by 1-2 cm in the SAOCOM DP, Sentinel-1 and SAOCOM QP datasets whereas the UAVSAR dataset showed an increase of around 7 cm in RMSE. The decrease in prediction accuracy implies that the model failed to generalize effectively when tested on an independent study area. The higher RMSE and MAE values can be attributed to the fact that the spatially disjoint region, Basin Summit, may have unique terrain characteristics that might have influenced SAR backscatter values and consequently affected the predicted snow depth. Moreover, the combined training dataset might also have included the noise or irrelevant variability from the training samples of the four study areas. The incorporation of noise could distort the model's understanding of the relations between SAR backscatter and snow depth measurements, which in turn could've affected the model's capacity to generalize to unseen data. Figure 15 shows the predicted snow depth maps produced during this investigation. diverse range of backscattering value.

4.4. Results of a complementary investigation of SDE using auxiliary data

To further investigate the impact of using auxiliary data for training the RF regression model, a complementary analysis was carried out on the Basin Summit region. During this stage, elevation data from the Copernicus 30m Digital Elevation Model (DEM) and SAR backscatter values both were used as predictor variables to train the models. The rest of the methodological workflow remained the same and the models were made to predict snow depth values for the study area. The objective of this additional investigation was to find out to what extent adding extra information, apart from SAR backscatter values, can affect the model's performance.

Table 7 shows the results of performance metrics comparing models trained with SAR data alone (Old RMSE and Old MAE) versus models built with a combination of SAR and DEM data (New RMSE and New MAE).

Table 7: Comparing the performance metrics of the model utilizing only SAR data and the model using SAR and DEM data

	RMSE		**MAE**	
Predictors	***SAR***	***SAR+DEM***	***SAR***	***SAR+DEM***
SACOM DP	0.549	0.459	0.400	0.282
Sentinel-1	0.540	0.420	0.388	0.232
SAOCOM QP	0.502	0.401	0.360	0.239
UAVSAR	0.438	0.358	0.327	0.195

The incorporation of DEM data led to a considerable reduction in both RMSE and MAE values for the Basin Summit region. For the SAOCOM DP dataset, the RMSE decreased from 0.54 m to 0.45 m, and the MAE decreased from 0.40 m to 0.28 m. Likewise, Sentinel-1 showed a

decrease in RMSE from 0.54 m to 0.42 m while the MAE decreased from 0.38 m to 0.23 m. The SAOCOM QP dataset also saw a reduction in RMSE from 0.50 m to 0.40 m, and the MAE also decreased from 0.36 m to 0.23 m. Notably, RMSE and MAE values experienced substantial improvement in the UAVSAR dataset, with RMSE falling from 0.43 m to 0.35 m and the MAE decreasing from 0.32 m to 0.19 m. These findings show that the inclusion of DEM data as a predictor variable significantly enhanced the accuracy of snow depth predictions using SAR data. The improved performance across all datasets indicates that integrating auxiliary data with SAR data has the potential to improve the predictive accuracy of a snow depth prediction model. It is essential to note that achieving high accuracies was not the primary objective of this research. Instead, the aim was to assess the reliability of SAR-based snow depth estimations and compare the performance of different SAR modalities. This additional investigation solely aimed at understanding the impact of adding an auxiliary dataset along with SAR to estimate snow depth using the same machine learning model. Figure 16 shows the predicted snow depth maps produced during this investigation. Upon visual inspection of these maps, it can be stated that the model trained with additional data was able to make better predictions because the predicted maps demonstrate much more closeness to the reference snow depth maps as compared to the predicted maps of Basin Summit using only SAR data.

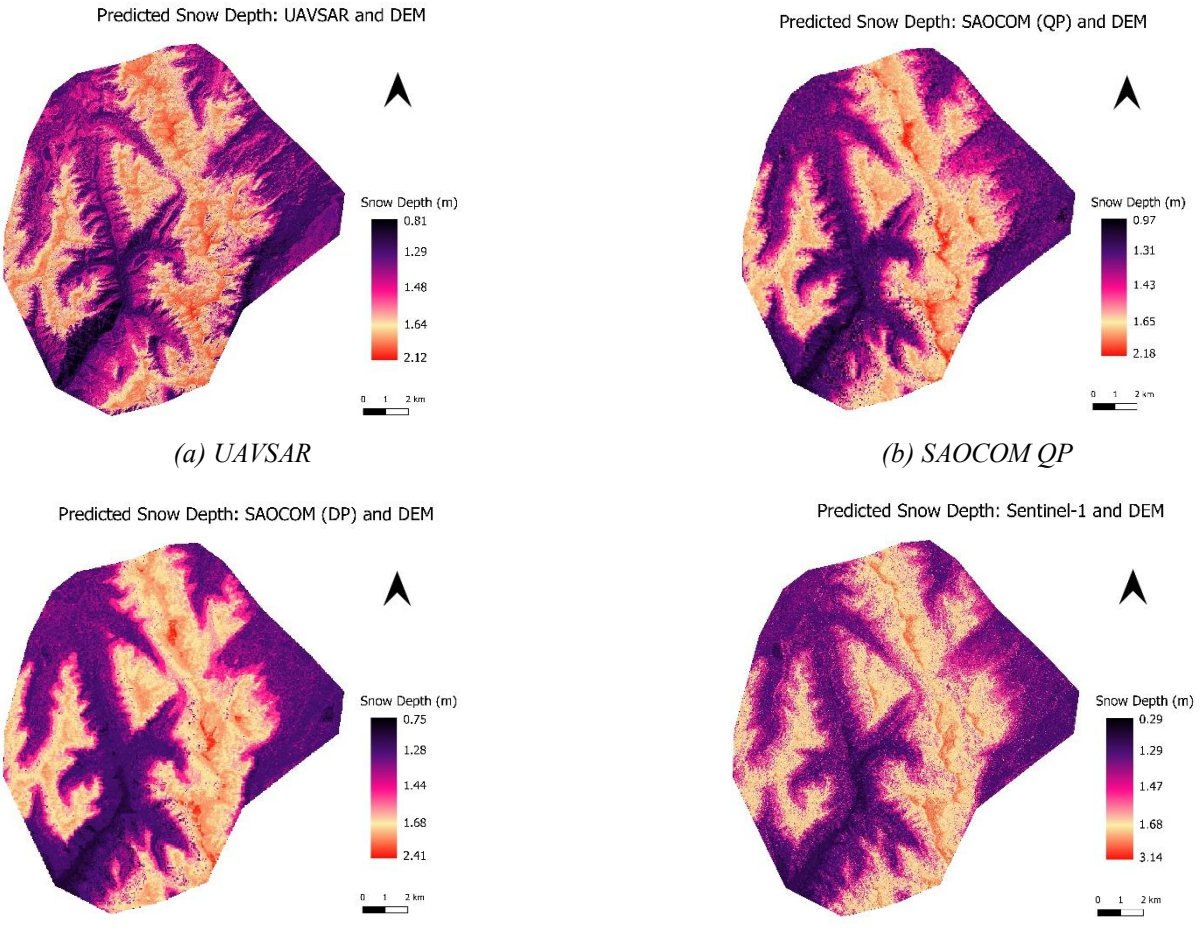

(a) UAVSAR *(b) SAOCOM QP*

(c) SAOCOM DP *(d) SENTINEL-1*

Figure 16: Predicted snow depth maps for the Basin Summit region, generated by training the models with additional DEM data: (a) UAVSAR, (b) SAOCOM (QP), (c) SAOCOM (DP), (d) Sentinel-1

CHAPTER 5

Conclusion

5.1. Answers to Research Questions

RQ1: Which frequency (C-band or L-band) of SAR results in a more accurate estimation of snow depth?

This question can be answered by comparing the performance of Sentinel-1 C- band and SAOCOM DP L- band datasets. Both datasets are dual-polarised and acquired from spaceborne sensors. The results revealed that the predictive accuracies of both the datasets were quite comparable. However, Sentinel-1 data performed slightly better than SAOCOM DP data, possibly due to its higher spatial resolution. Despite having a lower penetration capability than the L-band, the Sentinel-1 C-band data slightly outperformed in several cases. It suggests that although L-band's deeper penetration into the snowpack is advantageous, it may not be sufficient to make up for lower resolution when it comes to collecting details about snow depth. This implies that a higher spatial resolution has the potential to compensate for the less-penetrating C-band when estimating snow depth.

On the other hand, it is noteworthy that even though Sentinel-1 has a much higher resolution (10m) than SAOCOM DP (50m), the increase in accuracy for Sentinel-1 was not much. The RMSE and MAE values of Sentinel-1 were extremely close to the respective values of SAOCOM DP. The small difference between their performance metrics shows that L-band SAOCOM DP achieved nearly comparable accuracy in SDE despite having a poorer resolution.

Moreover, this comparison might not be entirely fair because of the disparity in spatial resolution between the two datasets. Thus, the answer to this question remains debatable. Future studies should consider datasets where all other features are held constant, except for frequency, in order to obtain a more precise assessment of the effect of frequency on SDE.

RQ2: Do the SDE accuracies differ across airborne SAR and spaceborne SAR when the same frequency (L-band) is used?

This question can be answered by comparing the performance of airborne UAVSAR and spaceborne SAOCOM QP datasets. Both datasets used quad-polarised configuration and L-band frequency. The results of this study revealed that UAVSAR consistently achieved lower RMSE and MAE values than the SAOCOM QP dataset. This superior performance of UAVSAR can be attributed to the sensor's high spatial resolution which could capture finer details. Airborne L-band SAR systems may also have an advantage over spaceborne L-band SAR systems due to their closer proximity to the Earth's surface which may allow for higher energy to penetrate the snowpack. Thus, an airborne SAR system should be preferred over a spaceborne one to achieve higher predictive accuracies in the context of SDE. However, it is

important to note that this higher accuracy of airborne systems comes with significantly higher costs associated with its operational expenses. On the contrary, the acquisition of satellite imagery from spaceborne systems is less expensive. Therefore, even if aerial SAR data offers more accuracy, its cost-effectiveness needs to be taken into account, particularly for large-scale or long-term snow monitoring studies.

RQ3: Which of the polarization modalities (full-polarization or dual-polarization) results in a more accurate estimation of snow depth?

The comparison of the SDE accuracies of SAOCOM'S DP and QP data can facilitate the answer to this question. While both datasets had the same spatial resolution and L-band frequency, the results of this study revealed that the QP data proved to be more accurate at predicting snow depth values. The DP data of SAOCOM contains information in two channels (VH, VV) while the QP data provides data in four channels (HH, HV, VH, VV). Thus, this additional information provided by QP data helped the machine learning model in better understanding the snowpack which led to its lower RMSE and MAE values across most study areas. Thus, SAOCOM QP clearly outperformed the SAOCOM DP dataset, indicating that QP SAR data is more advantageous over DP SAR data in the estimation of snow depth.

5.2. Uncertainties

While conducting this research, several sources of uncertainty were identified that could affect the accuracy and reliability of the snow depth predictions. Some amount of residual noise persists even after applying speckle filtering techniques which may impact the accuracy of snow depth estimations (Qiu et al., 2004). Additionally, there exists a gap of many days between the acquisition dates of the SAR data and reference data. This may lead to discrepancies because snow depth can change rapidly due to snow-melting or new snowfall over a period of a few days. Thus, temporal alignment between SAR data acquisitions and reference snow depth measurements is critical for accurate SDE. The original SAOCOM images were found to have geolocation errors due to which the pixels of the image were displaced from their true ground locations by a few metres. This led to misalignments between the SAOCOM data and the reference snow depth images. The inherent errors in GCP placement used for georeferencing may have introduced additional uncertainties. Since the georeferencing was done manually, there remains a possibility of persisting geo-location errors or imperfect alignment between the SAR images and their corresponding snow depth images. The original snow depth raster images used as reference data are also significant sources of uncertainty. These images were derived from point cloud DTMs, which might have involved interpolation of snow depth values. The exact extent of these uncertainties is unknown, adding another layer of complexity to the overall uncertainty in this research.

5.3. Implications

The accurate estimation of snow depth using SAR data holds significant implications across various sectors and applications due to its practical importance. Snow depth is essential for calculating snow water equivalent which is essential for communities reliant on snowmelt for

agriculture, drinking water, and hydropower generation. It is also vital for assessing flood risks associated with rapid snowmelt events, enabling authorities to anticipate and mitigate hazards, and enhancing disaster preparedness and response strategies. Snow depth information also supports the tourism industry, enabling ski resorts and recreational facilities to optimize operations, ensure visitor safety, and enhance visitor experience. Reliable assessments of snow depth are important for avalanche risk assessment and disaster management, identifying high-risk areas and informing proactive measures to mitigate hazards. Thus, accurate SDE has far-reaching potential for water resource management, flood prevention, tourism, and disaster risk reduction.

5.4. Future Work and Recommendations

In future, the study can incorporate phase information along with intensity information by making use of Single Look Complex (SLC) SAR data. Moreover, effective filtering techniques such as non-local or deep learning filters could be used (Aghababaei et al., 2022). Employing advanced techniques like Convolutional Neural Networks (CNNs) and Recurrent Neural Networks (RNNs) in future might prove to be effective at discerning complex patterns and relationships within SAR backscatter and snow depth values. Moreover, efforts can be made to refine the currently proposed methodology by tackling overfitting and improving sampling strategies. Additionally, integrating a variety of auxiliary data sources such as DEMs, thermal images, in-situ measurements, etc. can provide contextual insights that refine the connection between SAR-derived backscatter signals and variations in snow depth (Yang et al., 2020). These recommendations have the potential to advance the development of precise and dependable frameworks for estimating snow depth using SAR data.

5.5. Summary

This research explored the use of various SAR datasets to estimate snow depth across multiple study areas in the western United States. By using a machine learning model, namely Random Forest regression, the study evaluated the performance of different SAR modalities, including C-band and L-band frequencies, airborne and spaceborne platforms, and dual-polarimetric and full-polarimetric configurations. The UAVSAR dataset consistently yielded the most accurate snow depth estimates, followed by SAOCOM QP, Sentinel-1, and SAOCOM DP. The study revealed that the airborne platforms (UAVSAR) generally yield more accurate snow depth estimations due to higher resolution and closer proximity to the snowpack, than the spaceborne ones (SAOCOM QP). Moreover, fully-polarimetric SAR data (SAOCOM QP) is more effective than dual-polarimetric configurations (SAOCOM DP), as it provides additional information to the model. When comparing the effect of the frequency of radar signals, dual-polarised C-band data (Sentinel-1) showed better predictive accuracy than dual-polarised L-band data (SAOCOM DP), suggesting that a higher spatial resolution has the potential to compensate for the less-penetrating C-band when estimating snow depth. The study's findings have significant implications for hydrology, water resource management, disaster management, etc. Overall, this research establishes a strong foundation for assessing SAR-based snow depth estimations and understanding the potential of the most available SAR data resources on SDE.

5.6. Data Management

This study involved significant data management and storage requirements. Data was systematically arranged and stored, ensuring simple access throughout the research process. Data quality problems, one of the study's potential risks, were mitigated by data pre-processing methods. To prevent data loss, data redundancy was used, and frequent backups were made on a hard drive.

5.7. Ethical considerations

This research was conducted using data from dependable sources. The ITC Faculty of Geo-information Science and Earth Observation at the University of Twente received the SAOCOM-1A dataset with the explicit consent of the CONAE. This dataset is subject to certain usage restrictions; therefore, this data was only used for the goals described in this research. The data will not be disseminated to anyone else. The SnowEx20-21 QSI Lidar Snow Depth dataset from the NASA Open Data Portal and the Sentinel-1A dataset from the European Space Agency (ESA) are both publicly accessible. Similarly, the UAVSAR imagery was freely available on the official website of NASA's JPL. These publicly accessible datasets were also used solely for the objectives of this research, ensuring responsible use of these datasets. The contributions of additional authors were recognized per the standards of the American Psychological Association (APA) 7th edition referencing style. The results of this research do not contain any false information, and they were not skewed in any way.

5.8. Use of AI

The author utilized OpenAI's ChatGPT to grasp various concepts, that were later extensively studied by reliable and valid references. The content was additionally proofread for grammatical errors using Grammarly. The author examined and revised the content after utilizing these AI tools and services, taking full responsibility for the work's content.

REFERENCES

Adnan, R. M., Yuan, X., Kisi, O., & Yuan, Y. (n.d.). Streamflow Forecasting Using Artificial Neural Network and Support Vector Machine Models. *American Scientific Research Journal for Engineering*. Retrieved November 12, 2023, from http://asrjetsjournal.org/

Aghababaei, H., Ferraioli, G., Vitale, S., Zamani, R., Schirinzi, G., & Pascazio, V. (2022). Nonlocal Model-Free Denoising Algorithm for Single- and Multichannel SAR Data. *IEEE Transactions on Geoscience and Remote Sensing*, *60*. https://doi.org/10.1109/TGRS.2021.3127109

Atwood, D. K., Small, D., & Gens, R. (2012). Improving PolSAR land cover classification with radiometric correction of the coherency matrix. *IEEE Journal of Selected Topics in Applied Earth Observations and Remote Sensing*, *5*(3), 848–856. https://doi.org/10.1109/JSTARS.2012.2186791

Baños, I. M., García, A. R., Alavedra, J. M. I., Figueras, P. O. I., Iglesias, J. P., Figueras, P. M. I., & López, J. T. (2011). Assessment of airborne LIDAR for snowpack depth modeling. *Boletin de La Sociedad Geologica Mexicana*, *63*(1), 95–107. https://doi.org/10.18268/BSGM2011V63N1A8

Bashmakov, I. A., Nilsson, L. J., Acquaye, A., Bataille, C., Cullen, J. M., de la Rue du Can, S., Fischedick, M., Geng, Y., & Tanaka, K. (2022). *Climate Change 2022: Mitigation of Climate Change. Contribution of Working Group III to the Sixth Assessment Report of the Intergovernmental Panel on Climate Change, Chapter 11*. https://doi.org/10.2172/1973106

Beniston, M., Keller, F., & Goyette, S. (2003). Snow pack in the Swiss Alps under changing climatic conditions: An empirical approach for climate impacts studies. *Theoretical and Applied Climatology*, *74*(1–2), 19–31. https://doi.org/10.1007/S00704-002-0709-1/METRICS

Breiman, L. (2001). Random forests. *Machine Learning*, *45*(1), 5–32. https://doi.org/10.1023/A:1010933404324/METRICS

Broxton, P. D., van Leeuwen, W. J. D., & Biederman, J. A. (2019). Improving Snow Water Equivalent Maps With Machine Learning of Snow Survey and Lidar Measurements. *Water Resources Research*, *55*(5), 3739–3757. https://doi.org/10.1029/2018WR024146

Bühler, Y., Bebi, P., Christen, M., Margreth, S., Stoffel, L., Stoffel, A., Marty, C., Schmucki, G., Caviezel, A., Kühne, R., Wohlwend, S., & Bartelt, P. (2022). Automated avalanche hazard indication mapping on a statewide scale. *Natural Hazards and Earth System Sciences*, *22*(6), 1825–1843. https://doi.org/10.5194/NHESS-22-1825-2022

Bühler, Y., Marty, M., Egli, L., Veitinger, J., Jonas, T., Thee, P., & Ginzler, C. (2015). Snow depth mapping in high-alpine catchments using digital photogrammetry. *Cryosphere*, *9*(1), 229–243. https://doi.org/10.5194/TC-9-229-2015

Cannistra, A. F., Shean, D. E., & Cristea, N. C. (2021). High-resolution CubeSat imagery and machine learning for detailed snow-covered area. *Remote Sensing of Environment*, *258*. https://doi.org/10.1016/J.RSE.2021.112399

Che, T., Li, X., Jin, R., Armstrong, R., & Zhang, T. (2008). Snow depth derived from passive microwave remote-sensing data in China. *Annals of Glaciology*, *49*, 145–154. https://doi.org/10.3189/172756408787814690

Cheng, X., Naiara, P., & Gong, J. (2012). Terrain radiometric calibration of airborne UAVSAR for forested area. *Geo-Spatial Information Science*, *15*(4), 229–240. https://doi.org/10.1080/10095020.2012.745050
Cimoli, E., Marcer, M., Vandecrux, B., Bøggild, C. E., Williams, G., & Simonsen, S. B. (2017). Application of Low-Cost UASs and Digital Photogrammetry for High-Resolution Snow Depth Mapping in the Arctic. *Remote Sensing 2017, Vol. 9, Page 1144*, *9*(11), 1144. https://doi.org/10.3390/RS9111144
Currier, W. R., Pflug, J., Mazzotti, G., Jonas, T., Deems, J. S., Bormann, K. J., Painter, T. H., Hiemstra, C. A., Gelvin, A., Uhlmann, Z., Spaete, L., Glenn, N. F., & Lundquist, J. D. (2019). Comparing Aerial Lidar Observations With Terrestrial Lidar and Snow-Probe Transects From NASA's 2017 SnowEx Campaign. *Water Resources Research*, *55*(7), 6285–6294. https://doi.org/10.1029/2018WR024533
Das, R. K., Samanta, S., Jana, S. K., & Rosa, R. (2018). Polynomial interpolation methods in development of local geoid model. *The Egyptian Journal of Remote Sensing and Space Science*, *21*(3), 265–271. https://doi.org/10.1016/J.EJRS.2017.03.002
Daudt, R. C., Wulf, H., Hafner, E. D., Bühler, Y., Schindler, K., & Wegner, J. D. (2023). Snow depth estimation at country-scale with high spatial and temporal resolution. *ISPRS Journal of Photogrammetry and Remote Sensing*, *197*, 105–121. https://doi.org/10.1016/J.ISPRSJPRS.2023.01.017
De Leeuw, J., Jia, H., Yang, L., Liu, X., Schmidt, K., Skidmore, A. K., De Leeuw{, J., Jia{, H., Liu{, X., Schmidt{, K., & Skidmore{, A. K. (2006). Comparing accuracy assessments to infer superiority of image classification methods. *International Journal of Remote Sensing*, *27*(1), 223–232. https://doi.org/10.1080/01431160500275762
Deeb, E. J., Marshall, H. P., Forster, R. R., Jones, C. E., Hiemstra, C. A., & Siqueira, P. R. (2017). Supporting NASA SnowEx remote sensing strategies and requirements for L-band interferometric snow depth and snow water equivalent estimation. *International Geoscience and Remote Sensing Symposium (IGARSS)*, *2017-July*, 1395–1396. https://doi.org/10.1109/IGARSS.2017.8127224
Deems, J. S., Painter, T. H., & Finnegan, D. C. (2013). Lidar measurement of snow depth: a review. *Journal of Glaciology*, *59*(215), 467–479. https://doi.org/10.3189/2013JOG12J154
Domingos, P. (2012). A few useful things to know about machine learning. *Communications of the ACM*, *55*(10), 78–87. https://doi.org/10.1145/2347736.2347755
Eberhard, L. A., Sirguey, P., Miller, A., Marty, M., Schindler, K., Stoffel, A., & Bühler, Y. (2021). Intercomparison of photogrammetric platforms for spatially continuous snow depth mapping. *Cryosphere*, *15*(1), 69–94. https://doi.org/10.5194/TC-15-69-2021
El-Darymli, K., McGuire, P., Gill, E., Power, D., & Moloney, C. (2014). Understanding the significance of radiometric calibration for synthetic aperture radar imagery. *Canadian Conference on Electrical and Computer Engineering*. https://doi.org/10.1109/CCECE.2014.6901104
Filipponi, F. (2019). Sentinel-1 GRD Preprocessing Workflow. *Proceedings 2019, Vol. 18, Page 11*, *18*(1), 11. https://doi.org/10.3390/ECRS-3-06201
Fore, A. G., Chapman, B. D., Hawkins, B. P., Hensley, S., Jones, C. E., Michel, T. R., & Muellerschoen, R. J. (2015). UAVSAR polarimetric calibration. *IEEE Transactions on Geoscience and Remote Sensing*, *53*(6), 3481–3491. https://doi.org/10.1109/TGRS.2014.2377637
Gabriel, A. K. (2002). A simple model for SAR azimuth speckle, focusing, and interferometric decorrelation. *IEEE Transactions on Geoscience and Remote Sensing*, *40*(8), 1885–1889. https://doi.org/10.1109/TGRS.2002.802456

Gallet, J. C., Domine, F., Zender, C. S., & Picard, G. (2009). Measurement of the specific surface area of snow using infrared reflectance in an integrating sphere at 1310 and 1550 nm. *Cryosphere*, *3*(2), 167–182. https://doi.org/10.5194/TC-3-167-2009

Ghannadi, M. A., Alebooye, S., Izadi, M., & Ghanadi, A. (n.d.). *VERTICAL ACCURACY ASSESSMENT OF COPERNICUS DEM (CASE STUDY: TEHRAN AND JAM CITIES)*. https://doi.org/10.5194/isprs-annals-X-4-W1-2022-209-2023

Ghojogh, B., Ca, B., Crowley, M., & Ca, M. (2019). *The Theory Behind Overfitting, Cross Validation, Regularization, Bagging, and Boosting: Tutorial*. https://arxiv.org/abs/1905.12787v2

Guneriussen, T., HJgda, K. A., Johnsen, H., & Lauknes, I. (2001). InSAR for estimation of changes in snow water equivalent of dry snow. *IEEE Transactions on Geoscience and Remote Sensing*, *39*(10), 2101–2108. https://doi.org/10.1109/36.957273

Ha, J., Shin, D. H., Eun, J., Ahn, P., & Kim, J. (2018). Learning convolutional neural network using data from other domains in case of insufficient data. *ACM International Conference Proceeding Series*, 122–126. https://doi.org/10.1145/3209914.3209927

Hensley, S., Wheeler, K., Sadowy, G., Jones, C., Shaffer, S., Zebker, H., Miller, T., Heavey, B., Chuang, E., Chao, R., Vines, K., Nishimoto, K., Prater, J., Carrico, B., Chamberlain, N., Shimada, J., Simard, M., Chapman, B., Muellerschoen, R., … Smiths, R. (2008). The UAVSAR instrument: Description and first results. *International Radar Conference*. https://doi.org/10.1109/RADAR.2008.4720722

Hoppinen, Z., Oveisgharan, S., Marshall, H. P., Mower, R., Elder, K., & Vuyovich, C. (2024). Snow water equivalent retrieval over Idaho - Part 2: Using L-band UAVSAR repeat-pass interferometry. *Cryosphere*, *18*(2), 575–592. https://doi.org/10.5194/TC-18-575-2024

Hultquist, C., Chen, G., & Zhao, K. (2014). A comparison of Gaussian process regression, random forests and support vector regression for burn severity assessment in diseased forests. *Remote Sensing Letters*, *5*(8), 723–732. https://doi.org/10.1080/2150704X.2014.963733

Jones, C. E., Minchew, B., Holt, B., & Hensley, S. (2013). Studies of the Deepwater Horizon Oil Spill With the UAVSAR Radar. *Monitoring and Modeling the Deepwater Horizon Oil Spill: A Record Breaking Enterprise*, 33–50. https://doi.org/10.1029/2011GM001113

Karl, J. W. (2010). Spatial Predictions of Cover Attributes of Rangeland Ecosystems Using Regression Kriging and Remote Sensing. *Rangeland Ecology & Management*, *63*(3), 335–349. https://doi.org/10.2111/REM-D-09-00074.1

Kelly, R. E., Chang, A. T., Tsang, L., & Foster, J. L. (2003). A prototype AMSR-E global snow area and snow depth algorithm. *IEEE Transactions on Geoscience and Remote Sensing*, *41*(2 PART 1), 230–242. https://doi.org/10.1109/TGRS.2003.809118

Kittel, F., Thornton, P., Royle, A., & Chase, T. (2002). Climates of the Rocky Mountains: Historical and future patterns. *Rocky Mountain Futures: An Ecological Perspective*, 59–82. https://opensky.ucar.edu/islandora/object/books%3A460/

Kittel, T. G. F., Baker, B. B., Higgins, J. V., & Haney, J. C. (2011). Climate vulnerability of ecosystems and landscapes on Alaska's North Slope. *Regional Environmental Change*, *11*(SUPPL. 1), 249–264. https://doi.org/10.1007/S10113-010-0180-Y/FIGURES/7

Leinss, S., Parrella, G., & Hajnsek, I. (2014). Snow height determination by polarimetric phase differences in X-Band SAR Data. *IEEE Journal of Selected Topics in Applied Earth Observations and Remote Sensing*, *7*(9), 3794–3810. https://doi.org/10.1109/JSTARS.2014.2323199

Li, Y. ;, Zhao, X. ;, Zhao, Q., Li, Y., Zhao, X., & Zhao, Q. (2022). Snow Depth Inversion in Forest Areas from Sentinel-1 Data Based on Phase Deviation Correction. *Remote Sensing 2022, Vol. 14, Page 5930*, *14*(23), 5930. https://doi.org/10.3390/RS14235930

Lievens, H., Brangers, I., Marshall, H. P., Jonas, T., Olefs, M., & De Lannoy, G. (2022). Sentinel-1 snow depth retrieval at sub-kilometer resolution over the European Alps. *Cryosphere*, *16*(1), 159–177. https://doi.org/10.5194/TC-16-159-2022

Lievens, H., Demuzere, M., Marshall, H. P., Reichle, R. H., Brucker, L., Brangers, I., de Rosnay, P., Dumont, M., Girotto, M., Immerzeel, W. W., Jonas, T., Kim, E. J., Koch, I., Marty, C., Saloranta, T., Schöber, J., & De Lannoy, G. J. M. (2019). Snow depth variability in the Northern Hemisphere mountains observed from space. *Nature Communications 2019 10:1*, *10*(1), 1–12. https://doi.org/10.1038/s41467-019-12566-y

Marshall, H. P., Deeb, E., Forster, R., Vuyovich, C., Elder, K., Hiemstra, C., & Lund, J. (2021). L-BAND INSAR DEPTH RETRIEVAL DURING THE NASA SNOWEX 2020 CAMPAIGN: GRAND MESA, COLORADO. *International Geoscience and Remote Sensing Symposium (IGARSS)*, *2021-July*, 625–627. https://doi.org/10.1109/IGARSS47720.2021.9553852

Marshall, H. P., Vuyovich, C., Skiles, M., Sproles, E., Gleason, K., Elder, K., Gleason, A., Mcgrath, D., Hiemstra, C., Houser, P., & Cho, E. (n.d.). *NASA SnowEx 2021 Experiment Plan Draft (December 2020)*.

Maxwell, A. E., Warner, T. A., & Fang, F. (2018). Implementation of machine-learning classification in remote sensing: an applied review. *International Journal of Remote Sensing*, *39*(9), 2784–2817. https://doi.org/10.1080/01431161.2018.1433343

McGrath, D., Webb, R., Shean, D., Bonnell, R., Marshall, H. P., Painter, T. H., Molotch, N. P., Elder, K., Hiemstra, C., & Brucker, L. (2019). Spatially Extensive Ground-Penetrating Radar Snow Depth Observations During NASA's 2017 SnowEx Campaign: Comparison With In Situ, Airborne, and Satellite Observations. *Water Resources Research*, *55*(11), 10026–10036. https://doi.org/10.1029/2019WR024907

Montpetit, B., Royer, A., Langlois, A., Chum, M., Cliche, P., Roy, A., Champollion, N., & Picard, G. (2012). *In-situ Measurements for Snow Grain Size and Shape Characterization Using Optical Methods*.

Mou, J., Wang, Y., Hong, J., Wang, Y., Wang, A., Sun, S., & Liu, G. (2023). First Assessment of Bistatic Geometric Calibration and Geolocation Accuracy of Innovative Spaceborne Synthetic Aperture Radar LuTan-1. *Remote Sensing 2023, Vol. 15, Page 5280*, *15*(22), 5280. https://doi.org/10.3390/RS15225280

Muelchi, R., Rössler, O., Schwanbeck, J., Weingartner, R., & Martius, O. (2021). River runoff in Switzerland in a changing climate-runoff regime changes and their time of emergence. *Hydrology and Earth System Sciences*, *25*(6), 3071–3086. https://doi.org/10.5194/HESS-25-3071-2021

Muñoz-Sabater, J., Dutra, E., Agustí-Panareda, A., Albergel, C., Arduini, G., Balsamo, G., Boussetta, S., Choulga, M., Harrigan, S., Hersbach, H., Martens, B., Miralles, D. G., Piles, M., Rodríguez-Fernández, N. J., Zsoter, E., Buontempo, C., & Thépaut, J. N. (2021). ERA5-Land: A state-of-the-art global reanalysis dataset for land applications. *Earth System Science Data*, *13*(9), 4349–4383. https://doi.org/10.5194/ESSD-13-4349-2021

Painam, R. K., & Manikandan, S. (2023). BEMD based adaptive Lee filter for despeckling of SAR images. *Advances in Space Research*, *71*(8), 3140–3149. https://doi.org/10.1016/J.ASR.2022.12.009

Palomaki, R. T., & Sproles, E. A. (2023). Assessment of L-band InSAR snow estimation techniques over a shallow, heterogeneous prairie snowpack. *Remote Sensing of Environment*, *296*, 113744. https://doi.org/10.1016/J.RSE.2023.113744

Patil, A., Singh, G., & Rüdiger, C. (2020). Retrieval of Snow Depth and Snow Water Equivalent Using Dual Polarization SAR Data. *Remote Sensing 2020, Vol. 12, Page 1183*, *12*(7), 1183. https://doi.org/10.3390/RS12071183

Qiao, H., Zhang, P., Li, Z., Huang, L., Zhao, C., Gao, S., Liu, C., Wu, Z., Liang, S., Zhou, J., Sun, W., & Wang, L. (2023a). Snow profile reconstruction from tomographic UAV SAR. *International Journal of Applied Earth Observation and Geoinformation*, *118*, 103291. https://doi.org/10.1016/J.JAG.2023.103291

Qiao, H., Zhang, P., Li, Z., Huang, L., Zhao, C., Gao, S., Liu, C., Wu, Z., Liang, S., Zhou, J., Sun, W., & Wang, L. (2023b). Snow profile reconstruction from tomographic UAV SAR. *International Journal of Applied Earth Observation and Geoinformation*, *118*, 103291. https://doi.org/10.1016/J.JAG.2023.103291

Qiu, F., Berglund, J., Jensen, J. R., Thakkar, P., & Ren, D. (2004). *GIScience & Remote Sensing Speckle Noise Reduction in SAR Imagery Using a Local Adaptive Median Filter*. https://doi.org/10.2747/1548-1603.41.3.244

Rodriguez-Galiano, V., Sanchez-Castillo, M., Chica-Olmo, M., & Chica-Rivas, M. (2015). Machine learning predictive models for mineral prospectivity: An evaluation of neural networks, random forest, regression trees and support vector machines. *Ore Geology Reviews*, *71*, 804–818. https://doi.org/10.1016/J.OREGEOREV.2015.01.001

Rosen, P. A., Hensley, S., Wheeler, K., Sadowy, G., Miller, T., Shaffer, S., Muellerschoen, R., Jones, C., Zebker, H., & Madsen, S. (2006). Uavsar: A new NASA airborne SAR system for science and technology research. *IEEE National Radar Conference - Proceedings*, 22–29. https://doi.org/10.1109/RADAR.2006.1631770

Saha, S., Moorthi, S., Pan, H. L., Wu, X., Wang, J., Nadiga, S., Tripp, P., Kistler, R., Woollen, J., Behringer, D., Liu, H., Stokes, D., Grumbine, R., Gayno, G., Wang, J., Hou, Y. T., Chuang, H. Y., Juang, H. M. H., Sela, J., … Goldberg, M. (2010). The NCEP Climate Forecast System Reanalysis. *Bulletin of the American Meteorological Society*, *91*(8), 1015–1058. https://doi.org/10.1175/2010BAMS3001.1

Salma, S., Keerthana, N., & Dodamani, B. M. (2022). Target decomposition using dual-polarization sentinel-1 SAR data: Study on crop growth analysis. *Remote Sensing Applications: Society and Environment*, *28*, 100854. https://doi.org/10.1016/J.RSASE.2022.100854

Schweizer, J., Jamieson, J. B., & Schneebeli, M. (2003). Snow avalanche formation. *Reviews of Geophysics*, *41*(4). https://doi.org/10.1029/2002RG000123

Segal, M. R. (2004). *UCSF Recent Work Title Machine Learning Benchmarks and Random Forest Regression Publication Date Machine Learning Benchmarks and Random Forest Regression*.

Seo, D. K., Kim, Y. H., Eo, Y. D., Lee, M. H., & Park, W. Y. (2018). Fusion of SAR and Multispectral Images Using Random Forest Regression for Change Detection. *ISPRS International Journal of Geo-Information 2018, Vol. 7, Page 401*, *7*(10), 401. https://doi.org/10.3390/IJGI7100401

Singh, P., & Shree, R. (2016). Analysis and effects of speckle noise in SAR images. *Proceedings - 2016 International Conference on Advances in Computing, Communication and Automation (Fall), ICACCA 2016*. https://doi.org/10.1109/ICACCAF.2016.7748978

SnowEx20-21 QSI Lidar Snow Depth 3m UTM Grid, Version 1 | National Snow and Ice Data Center. (n.d.). Retrieved June 20, 2024, from https://nsidc.org/data/snex20_qsi_sd_3m/versions/1

Sospedra-Alfonso, R., Melton, J. R., & Merryfield, W. J. (2015). Effects of temperature and precipitation on snowpack variability in the Central Rocky Mountains as a function

of elevation. *Geophysical Research Letters*, *42*(11), 4429–4438. https://doi.org/10.1002/2015GL063898
Spadavecchia, L., & Williams, M. (2009). Can spatio-temporal geostatistical methods improve high resolution regionalisation of meteorological variables? *Agricultural and Forest Meteorology*, *149*(6–7), 1105–1117. https://doi.org/10.1016/J.AGRFORMET.2009.01.008
Tedesco, M., Derksen, C., Deems, J. S., & Foster, J. L. (2014). Remote sensing of snow depth and snow water equivalent. *Remote Sensing of the Cryosphere*, 73–98. https://doi.org/10.1002/9781118368909.CH5
Tyralis, H., Papacharalampous, G., & Tantanee, S. (2019). How to explain and predict the shape parameter of the generalized extreme value distribution of streamflow extremes using a big dataset. *Journal of Hydrology*, *574*, 628–645. https://doi.org/10.1016/J.JHYDROL.2019.04.070
Ulaby, F. T., & Long, D. G. (2015). Microwave Radiometry and Radiative Transfer. *Microwave Radar and Radiometric Remote Sensing*, 226–261.
Varade, D., & Dikshit, O. (2018). *Commission V, SS: Natural Resources Management*. https://doi.org/10.5194/isprs-annals-IV-5-223-2018
Varade, D., & Dikshit, O. (2019). Potential of multispectral reflectance for assessment of snow geophysical parameters in Solang valley in the lower Indian Himalayas. *Https://Doi.Org/10.1080/15481603.2019.1672365*, *57*(1), 107–126. https://doi.org/10.1080/15481603.2019.1672365
Varade, D., Maurya, A. K., Dikshit, O., Singh, G., & Manickam, S. (2019). Snow depth in Dhundi: an estimate based on weighted bias corrected differential phase observations of dual polarimetric bi-temporal Sentinel-1 data. *Https://Doi.Org/10.1080/01431161.2019.1698076*, *41*(8), 3031–3053. https://doi.org/10.1080/01431161.2019.1698076
Varade, D., Maurya, A. K., Dikshit, O., Singh, G., & Manickam, S. (2020). Snow depth in Dhundi: an estimate based on weighted bias corrected differential phase observations of dual polarimetric bi-temporal Sentinel-1 data. *International Journal of Remote Sensing*, *41*(8), 3031–3053. https://doi.org/10.1080/01431161.2019.1698076
Vikhamar, D., & Solberg, R. (2003). Subpixel mapping of snow cover in forests by optical remote sensing. *Remote Sensing of Environment*, *84*(1), 69–82. https://doi.org/10.1016/S0034-4257(02)00098-6
Worby, A. P., Markus, T., Steer, A. D., Lytle, V. I., & Massom, R. A. (2008). Evaluation of AMSR-E snow depth product over East Antarctic sea ice using in situ measurements and aerial photography. *Journal of Geophysical Research: Oceans*, *113*(C5), 5–94. https://doi.org/10.1029/2007JC004181
Wulf, H., Sassik, B., Milani, G., & Leiterer, R. (2020). High-resolution snow depth monitoring for entire mountain ranges. *Proceedings - 2020 7th Swiss Conference on Data Science, SDS 2020*, 41–46. https://doi.org/10.1109/SDS49233.2020.00008
Yang, J., Jiang, L., Luojus, K., Pan, J., Lemmetyinen, J., Takala, M., & Wu, S. (2020). Snow depth estimation and historical data reconstruction over China based on a random forest machine learning approach. *Cryosphere*, *14*(6), 1763–1778. https://doi.org/10.5194/TC-14-1763-2020
Zebker, H. A., Rosen, P. A., & Hensley, S. (1997). Atmospheric effects in interferometric synthetic aperture radar surface deformation and topographic maps. *Journal of Geophysical Research: Solid Earth*, *102*(B4), 7547–7563. https://doi.org/10.1029/96JB03804

Zhou, L., Xu, S., Liu, J., & Wang, B. (2018). On the retrieval of sea ice thickness and snow depth using concurrent laser altimetry and L-band remote sensing data. *The Cryosphere*, *12*, 993–1012. https://doi.org/10.5194/tc-12-993-2018